



Multi-model study of mercury dispersion in the atmosphere: Vertical distribution of mercury species

Johanes Bieser^{1,2}, Franz Slemr³, Jesse Ambrose⁴, Carl Brenningmeijer³, Steve
5 Brooks^{5,6}, Ashu Dastoor⁷, Francesco DeSimone⁸, Ralf Ebinghaus¹, Christian N.
Gencarelli⁸, Beate Geyer¹, Lynne E. Gratz⁹, Ian M. Hedgecock⁸, Daniel Jaffe^{4,10}, Paul
Kelley^{5,11}, Che-Jen Lin¹², Volker Matthias¹, Andrei Ryjkov⁷, Noelle E. Selin^{13,14},
Shaojie Song¹³, Oleg Travnikov¹⁵, Andreas Weigelt^{1,16}, Winston Luke⁵, Xinrong
Ren^{5,11,17}, Andreas Zahn¹⁸, Xin Yang¹⁹, Yun Zhu²⁰, Nicola Pirrone²¹

10

- 1 *Helmholtz Zentrum Geesthacht, 21052 Geesthacht, Germany*
- 2 *DLR – Deutsches Luft und Raumfahrtzentrum, Münchener Straße 20, 82234 Weßling, Germany*
- 3 *Max-Planck-Institute for Chemistry (MPI), Hahn-Meitner-Weg 1, 55128 Mainz, Germany*
- 4 *School of Science, Technology, Engineering and Mathematics, University of Washington-Bothell, Bothell, WA, USA*
- 15 5 *Air Resources Laboratory, National Oceanic and Atmospheric Administration, 5830 University Research Court, College Park, MD 20740, USA*
- 6 *Department of Mechanical, Aerospace and Biomedical Engineering, University of Tennessee Space Institute, 411 BH Goethert Parkway, Tullahoma, TN 37388, USA*
- 7 *ECCC – Air Quality Research Division, Environment and Climate Change Canada, Dorval, Canada*
- 20 8 *CNR-Institute of Atmospheric Pollution Research, Division of Rende, Rende, Italy*
- 9 *Environmental Program, Colorado College, Colorado Springs, CO, USA*
- 10 *School of Science, Technology, Engineering and Mathematics, University of Washington-Bothell, Bothell, WA, USA*
- 11 *Cooperative Institute for Climate and Satellites, University of Maryland, 5825 University Research Court, College Park, MD 20740, USA*
- 25 12 *Center for Advances in Water and Air Quality, Lamar University, Beaumont, Texas, USA.*
- 13 *Department of Earth, Atmospheric and Planetary Sciences, Massachusetts Institute of Technology, Cambridge, MA, USA*
- 14 *Institute for Data, Systems, and Society, Massachusetts Institute of Technology, Cambridge, MA, USA*
- 15 *Meteorological Synthesizing Centre – East of EMEP, Moscow, Russia*
- 16 *Federal Maritime and Hydrographic Agency (BSH), Hamburg, Germany*
- 30 17 *Department of Earth, Ocean, and Atmospheric Science, Florida State University, 117 North Woodward Avenue, Tallahassee, FL 32306, USA*
- 18 *Institut für Meteorologie und Klimaforschung (IMK-ASF), Karlsruhe Institut für Technologie, Hermann-von-Helmholtz-Platz 1, 76344 Leopoldshafen, Germany*
- 19 *British Antarctic Survey, Cambridge, UK*
- 35 20 *South China University of Technology, School of Environment and Energy, Guangzhou, China*
- 21 *CNR Institute of Atmospheric Pollution Research, Rome, Italy*



Abstract

Atmospheric chemistry and transport of mercury play a key role in the global mercury cycle. However, there are still considerable knowledge gaps concerning the fate of mercury in the atmosphere. This is the second part of a model inter-comparison study investigating the impact of atmospheric chemistry and emissions on mercury in the atmosphere. While the first study focused on ground based observations of mercury concentration and deposition, here we investigate the vertical distribution and speciation of mercury from the planetary boundary layer to the lower stratosphere. So far, there have been few model studies investigating the vertical distribution of mercury, mostly focusing on single aircraft campaigns. Here, we present a first comprehensive analysis based on various aircraft observations in Europe, North America, and on inter-continental flights.

The investigated models proved to be able to reproduce the distribution of total and elemental mercury concentrations in the troposphere including inter-hemispheric trends. One key aspect of the study is the investigation of mercury oxidation in the troposphere. We found that different chemistry schemes were better at reproducing observed oxidized mercury (RM) patterns depending on altitude. High RM concentrations in the upper troposphere could be reproduced with oxidation by bromine while elevated concentrations in the lower troposphere were better reproduced by OH and ozone chemistry. However, the results were not always conclusive as the physical and chemical parameterizations in the chemistry transport models also proved to have a substantial impact on model results.



1. Introduction

At the time of writing the Minamata Convention has 128 signatories and has been ratified by 35 countries.

- 65 This international legally binding treaty will oblige all participating parties to:
- I) Assess the state of mercury pollution
 - II) Take actions to reduce mercury emissions and concentrations in the environment
 - III) Evaluate the success of the measures taken on a regular basis.

70

The state of mercury contamination is typically determined by measurement of the relevant mercury species (e.g. total mercury in the atmosphere, methylmercury in fish). However, in order to understand the sources of mercury pollution and to predict the impact of various possible measures for mercury emission reduction it is necessary to apply complex chemistry transport models.

75

In the last decades, general chemistry transport models (CTMs) have been extended to model the global mercury cycle by including mercury chemistry and partitioning (Bergan et al., 1999; Xu et al., 2000; Lee et al., 2001; Peterson et al., 2001, Seigneur et al., 2001; Dastoor et al., 2004; Selin et al., 2007). Since then, extensive model inter-comparison studies have been performed to evaluate and improve the original models (Bullock et al., 2008; Ryaboshapko et al., 2007). However, up until today, we have not fully understood all parts of the global mercury cycle. In the atmosphere, the main question is how elemental mercury emitted from anthropogenic, natural, and legacy sources and then oxidized. This includes the relative importance of oxidizing reaction partners and the possibility of reduction pathways of oxidized mercury. Once we understand the red-ox processes of atmospheric mercury, is it possible to determine the range of mercury transport and the fate of mercury emitted in the past and the future.

80

85

Consequently, mercury oxidation processes have been in the focus of the international mercury community in recent years (Cohen et al., 2016; Amos et al., 2015; Dastoor et al., 2015; Song et al., 2015; Bieser et al., 2014; De Simone et al.,

90



2014; Qureshi et al., 2011; Travnikov et al., 2010).

In this study, we investigate the vertical distribution of mercury species in the atmosphere. While gaseous elemental mercury (GEM) makes up the vast majority
95 of total atmospheric mercury near the surface (Sprovieri et al., 2016 this issue), recent aircraft based observations have indicated that there is significant oxidation of mercury occurring in the free troposphere (Brooks et al., 2014; Jaffe and Lyman, 2012; Jaffe et al., 2014; Gratz et al., 2014; Shah et al., 2015). As gaseous oxidized mercury (GOM) is much more rapidly removed from the
100 atmosphere than elemental mercury the free troposphere, the region between the planetary boundary layer and the tropopause is of great importance for the global mercury budget.

To investigate this issue further, the Mercury Modelling Task Force (MMTF) was founded during the course of the EU FP7 project GMOS (Global Mercury
105 Observation System). The MMTF is a global collaboration, not limited to GMOS project partners and thus, incorporates most mercury CTMs currently in use in the scientific community. With a total of seven model combinations (including four global, one hemispheric, and two regional models), the partners in the MMTF carried out a set of sensitivity model runs and compared the results to airborne
110 observations in Europe, North America, and on intercontinental flights.

2. Methods

2.1 Observations

115 Aircraft based observations are expensive and thus rarely performed on a regular basis. They are made in a certain area at a limited time interval and as such are hardly representative enough to be used to evaluate model performance. However, in the year 2013 an unprecedented amount of aircraft based observations has been made:

120 Within the European Tropospheric Mercury Experiment (ETMEP) 5 vertical profiles were flown in the planetary boundary layer (PBL) and the lower free troposphere (LFT) at an altitude of 500 - 3500m over central Europe during



August 2013 (Weigelt et al., 2016a). Mercury was measured using two Tekran instruments (2537X and 2537B). Both Tekran instruments were run with upstream
125 particle filters and one, additionally, with a quartz wool trap which presumably removes gaseous oxidized mercury (GOM) (Lyman and Jaffe, 2011; Ambrose et al., 2013). Neglecting PBM the concentrations of which is usually negligible, the measurement by Tekran without the quartz wool trap approximates TM and that with quartz wool trap GEM (Weigelt et al., 2016b). GEM was also measured by a
130 modified Lumex instrument (Weigelt et al., 2016b). Additionally, gaseous oxidized mercury (GOM) was collected on denuders and analyzed on return to the laboratory.

In the U.S. Brooks et al. (2014) measured GEM, GOM, and PBM (particulate bound mercury) profiles on 28 flights between August 2012 and July 2013 at
135 altitudes from 1000m to 6000m. GEM was measured on board with a modified Tekran 2537B instrument with a temporal resolution of 2.5 minutes. GOM was collected on denuders and PBM on a filter tube downstream of the denuder. Both were later analyzed in the laboratory. In addition, 19 flights were flown in June and July 2013 mostly over the south-eastern USA at altitudes between 500m - 7000m
140 during the NOMADSS (Nitrogen, Oxidants, Mercury and Aerosol Distributions, Sources and Sinks) campaign (Gratz et al., 2015; Shah et al., 2016). Here, oxidized mercury was calculated based on a differential method using two Tekran 2537B instruments, one of which was equipped with GOM trap (quartz wool or ion-exchange membrane (DOHGS) (Lyman and Jaffe, 2011; Ambrose et al., 2015).
145 Finally, there were 19 intercontinental flights between Germany and North and South America were made within the CARIBIC (Civil Aircraft for the Regular Investigation of the atmosphere Based on an Instrumented Container) project during which TM and GEM was measured in the upper troposphere and the lower stratosphere in altitudes between 6000m - 12000m using a modified Tekran 2537
150 A instrument (Slemr et al., 2014; 2016).

The aircraft observations were complemented with ground based observations from the GMOS measurement network (Sprovieri et al., 2016; GMOS, 2016). In particular, we used data from the ground based stations in Mace Head, Ireland



and Waldhof, Germany to augment the ETMEP profiles (Weigelt et al., 2013;
155 2014). At Mace Head and Waldhof GEM is measured with a Tekran 2537 A. At
Waldhof, additionally, GOM and PBM are measured with a Tekran 1130/1135
speciation unit.

2.2 Models

160 This study is based on an ensemble of seven different CTMs including global
(GLEMOS, GEOS-Chem, GEM-MACH-Hg, ECHMERIT), hemispheric (CMAQ-Hem),
and regional (WRF-Chem, CCLM-CMAQ) models (Table 1). The models differ
considerably in the implemented physical and chemical parameterizations, spatial
and temporal resolution, and meteorological drivers. The ensemble includes
165 models that use external fields for chemical reaction partners (GLEMOS, GEOS-
Chem), models with a complete photochemical reaction scheme (CCLM-CMAQ,
CMAQ-Hem) and on-line coupled meteorological models (GEM-MACH-Hg,
ECHMERIT, WRF-Chem). The only model harmonization in this study is the
utilization of a common global 1°x1° anthropogenic emission inventory
170 (AMAP/UNEP, 2013a; 2013b). However, the models use different temporal
disaggregation and down-scaling methods, source heights, and speciation
schemes to convert the global emission dataset into model ready input fields. The
main analysis of the vertical mercury distribution was performed using the
standard setup of each model (BASE case). The chemical mechanisms for mercury
175 oxidation in the BASE case can be grouped into three major classes:

1) Ozone and OH chemistry (GLEMOS, ECHMERIT, CMAQ-Hem, CCLM-
CMAQ, WRF-Chem)

2) OH and bromine chemistry (GEM-MACH-Hg)

180 3) Bromine chemistry (GEOS-Chem)

Moreover, some models also consider reduction of Hg²⁺ to GEM in the aqueous
phase (GLEMOS, ECHMERIT, WRF-Chem, CMAQ). In addition to the BASE cases, a
set of chemistry and emission sensitivity runs was performed. These include runs



185 with no anthropogenic emissions (NOANT) and with a 100% GEMspeciation of
anthropogenic emissions (ANTSPEC). For the mercury chemistry, different runs
with only one of the above mentioned oxidants (OHCHEM, O3CHEM, BRCHEM) and
without any mercury chemistry (NOCHEM) were performed. Concerning the
bromine reaction, two different Br and BrO fields were used. These are bromine
190 fields from GEOS-Chem (Parella et al., 2012) and the p-TOMCAT model (Yang et al.,
2005, 2010). However, the described sensitivity runs were not performed by all
models. Moreover, the list differs from that published by Travnikov et al. (2016,
this issue) as only a limited set of 3D model output data could be saved. A
synthetic model description is given in Table 1 and the sensitivity runs performed
195 are further described in Table 2. An evaluation of ground based mercury
concentrations and deposition fluxes for the four global models (GLEMOS, GEOS-
Chem, GEM-MACH-Hg, ECHMERIT) can be found in Travnikov et al. (2016, this
issue). An evaluation of regional deposition fields can be found in Gencarelli et al.
(2016, this issue). For the sake of completeness we provide the detailed model
200 descriptions here as well.

2.2.1 GLEMOS

GLEMOS (Global EMEP Multi-media Modelling System) is a multi-scale chemistry
transport model developed for the simulation of environmental dispersion and
205 cycling of different chemicals including mercury based on the older hemispheric
model MSCE-HM-Hem (Travnikov, 2005; Travnikov and Ilyin, 2009; Travnikov et al.,
2009). The model simulates atmospheric transport, chemical transformations and
deposition of three Hg species (GEM, GOM and PBM). The atmospheric transport
of the tracers is driven by meteorological fields generated with the Weather
210 Research and Forecast modelling system (WRF 3.7.2) (Skamarock et al., 2007)
which is fed by operational analysis data from the European Centre for Medium-
Range Weather Forecast (ECMWF) (ECMWF, 2016). In the base configuration the
model grid has a horizontal resolution of $1^\circ \times 1^\circ$. Vertically, the model domain
reaches up to 10 hPa and consists of 20 irregular terrain-following sigma layers.
215 The atmospheric chemical scheme includes Hg oxidation and reduction reactions



in both the gas phase and the aqueous phase of cloud water. The major chemical mechanisms in the gas phase include Hg oxidation by O₃ and OH radicals with reaction rate constants taken from Hall (1995) and Sommar et al. (2001), respectively. The latter was scaled down by a factor of 0.1 within and below clouds
220 to account for reduced photochemical activity (Seigneur et al., 2001). The O₃ and OH concentration fields are imported from MOZART (Emmons et al., 2010). A two-step gas-phase oxidation of GEM by Br is included as an option. Aqueous-phase reactions include oxidation by ozone, chlorine and hydroxyl radical and reduction via decomposition of sulphite complexes (Van Loon et al. 2000). The model
225 distinguishes in-cloud and sub-cloud wet deposition of PBM and GOM based on empirical data. The dry deposition scheme is based on the resistance analogy approach (Wesely and Hicks, 2000). Prescribed fluxes of natural and secondary emissions of Hg from soil and seawater were generated depending on Hg concentrations in soil, soil temperature and solar radiation for emissions from land
230 and proportional to the primary production of organic carbon in seawater for emissions from the ocean (Travnikov and Ilyin, 2009). In addition, an empirical parametrization of the prompt Hg re-emission from snow- and ice-covered surfaces is applied based on observational data.

235 2.2.2 GEOS-Chem

The GEOS-Chem global chemistry transport model (v9-02; www.geos-chem.org) is driven by assimilated meteorological data from the NASA GMAO Goddard Earth Observing System (Bey et al., 2001). The GEOS-FP and GEOS-5.2.0 data are used for the simulation year 2013 and the spin-up period, respectively
240 (<http://gmao.gsfc.nasa.gov/products/>). GEOS-Chem couples a 3-D atmosphere (Holmes et al., 2010), a 2-D mixed layer slab ocean (Soerensen et al., 2010), and a 2-D terrestrial reservoir (Selin et al., 2008) in a horizontal resolution of 2°×2.5°. Three mercury species (GEM, GOM, and PBM) are tracked in the atmosphere (Amos et al., 2012). A two-step gaseous oxidation mechanism initialized by Br
245 atoms is used. Bromine fields are archived from a full-chemistry GEOS-Chem simulation (Parrella et al., 2012) while the rate constants of reactions are from



Goodsite et al. (2012), Donohoue et al. (2006), and Balabanov et al. (2005). The surface fluxes of GEM include anthropogenic sources, biomass burning, geogenic activities, as well as the bidirectional fluxes in the atmosphere-terrestrial and atmosphere-ocean exchanges (Song et al., 2015). Biomass burning emissions are estimated using a global CO emission database and a volume ratio of Hg/CO of 1×10^{-7} . Geogenic activities are spatially distributed based on the locations of mercury mines. For atmosphere-terrestrial exchange, GEOS-Chem treats the evasion and dry deposition of GEM separately (Selin et al., 2008). Dry deposition is parametrized with a resistance-in-series scheme (Wesely, 1989). In addition, an effective GOM uptake by sea-salt aerosol is also included over the ocean (Holmes et al., 2010). GEM evasion includes volatilization from soil and rapid recycling of newly deposited Hg. The former is estimated as a function of soil Hg content and solar radiation. The latter is modeled by recycling a fraction of wet/dry deposited oxidized mercury to the atmosphere as GEM immediately after deposition (60% for snow covered land and 20% for all other land uses) (Selin et al., 2008). GEOS-Chem estimates the atmosphere-ocean exchange of GEM using a standard two-layer diffusion model. The ocean mercury in the mixed layer interacts not only with the atmospheric boundary layer but also with subsurface waters through entrainment/detrainment of the mixed layer and wind-driven Ekman pumping (Soerensen et al., 2010).

2.2.3 GEM-MACH-Hg

GEM-MACH-Hg is a new chemical transport model for mercury that is based on the GRAHM model developed by Environment and Climate Change Canada (Dastoor et al., 2004; 2008; 2010; Durnford et al., 2010; 2012; Kos et al., 2013) GEM-MACH-Hg uses a newer version of the Environment and Climate Change Canada's operational meteorological model. The horizontal resolution of the model is $1^\circ \times 1^\circ$. GEM is oxidized in the atmosphere by OH radicals. The rate constant of the reaction is from Sommar et al. (2001), but scaled down by a coefficient of 0.34 to take into account possible dissociation/reduction reactions (Tossell et al., 2003; Goodsite et al., 2004). The gaseous oxidation of mercury by bromine is applied in



polar regions using reaction rate constants from Donohoue et al. (2006), Dibble et al. (2012) and Goodsite et al. (2004). The parametrization of atmospheric mercury
280 depletion events is based on Br production and chemistry, and snow re-emission of GEM (Dastoor et al., 2008).

OH fields are from MOZART (Emmons et al., 2010) while BrO is derived from 2007-2009 satellite observations of BrO vertical columns. The associated Br concentration is then calculated from photochemical steady state conditions (Platt
285 and Janssen, 1995). Dry deposition in GEM-MACH-Hg is based on the resistance approach (Zhang, 2001; Zhang et al., 2003). In the wet deposition scheme, GEM and GOM are partitioned between cloud droplets and air using a temperature-dependent Henry's law constant. Total global emissions from natural sources and re-emissions of previously deposited Hg (from land and oceans) in GEM-MACH-Hg
290 are based on the global Hg budgets by Gbor et al. (2007), Shetty et al. (2008) and Mason (2009). Land-based natural emissions are spatially distributed according to the natural enrichment of Hg. Terrestrial re-emissions are spatially distributed according to the historic deposition of Hg and land-use type and depend on solar radiation and the leaf area index. Oceanic emissions depend on the distributions
295 of primary production and atmospheric deposition.

2.2.4 ECHMERIT

ECHMERIT is a global on-line meteorological chemistry transport model, based on the ECHAM5 global circulation model, with a highly flexible chemistry mechanism
300 designed to facilitate the investigation of atmospheric mercury chemistry (Jung et al., 2009; De Simone et al., 2014, 2015, 2016). The model uses the same spectral grid as ECHAM. The standard horizontal resolution of the model is T42 (approximately, $2.8^{\circ} \times 2.8^{\circ}$), whereas in the vertical the model is discretized with a hybrid-sigma pressure system with 19 non-equidistant levels up to 10 hPa. The
305 base chemical mechanism includes the GEM oxidation by OH and O₃ in the gaseous and aqueous phases. Reaction rate constants are from Sommar et al. (2001), Hall (1995), and Munthe (1992), respectively. OH and O₃ concentration fields were imported from MOZART (Emmons et al., 2010). The Hg oxidation by Br



is also optionally available in a two-step gas phase oxidation mechanism with
310 reaction rates as described in Goodsite et al. (2004), Goodsite et al. (2012) and
Donohoue et al. (2006). ECHMERIT uses a parametrization of dynamic air-
seawater exchange as a function of ambient parameters, but using a constant
value of mercury concentration in seawater (De Simone et al., 2014). Emissions
from soils and vegetation were calculated off-line and derived from the
315 EDGAR/POET emission inventory (Granier et al., 2005; Peters and Olivier, 2003)
that includes biogenic emissions from the GEIA inventories
(<http://www.geiacenter.org>), as described by Jung et al. (2009). Prompt re-
emission of a fixed fraction (20%) of wet and dry deposited mercury is applied in
the model to account for reduction and evasion processes which govern mercury
320 short-term cycling between the atmosphere and terrestrial reservoirs (Selin et al.,
2008). This fraction is increased to 60% for snow-covered land and ice covered
seas.

2.2.5 CMAQ-Hem

325 This is a hemispheric set-up of the Community Multi-Scale Air Quality System
(CMAQ) version 4.6 (Byun and Schere, 2006; Byun and Ching, 1999). The model is
based on a three-dimensional Eulerian atmospheric chemistry and transport
modeling system that simulates Hg, ozone, particulate matter, acid deposition,
and visibility simultaneously. The model components and scientific backgrounds
330 have been documented elsewhere (Bullock and Brehme, 2002; Bullock et al.,
2008; Travnikov et al., 2010). A spin-up period of 10 days is used to eliminate the
impact of initial conditions for atmospheric oxidants (O_3 and OH) that react with
mercury. As for mercury species, global models were simulated for several years
prior to the study period (2005) in order to provide the initial and boundary
335 conditions for this study (Pongprueksa et al., 2011). A hemispheric model domain
with a Polar Stereographic projection at 108-km spatial resolution and 187×187
grid cells was used for this experiment with 13 sigma hybrid layers up to 50 hPa.
Hourly meteorological data were prepared using the Weather Research and
Forecasting (WRF) model Version 3.7 (Skamarock et al., 2008). The selected



340 physics options were Thompson (Microphysics Options) (Thompson et al., 2004),
Betts-Miller-Janjic (Cumulus Parameterization Options) (Janjic, 1994; 2000), RRTMG
(Radiation Physics Options) and BouLac (PBL Physics Options) based on the results
of meteorological model performance evaluation (Wang et al., 2014). The ARW
345 outputs were processed using MCIPv3.4.1 (Byun and Ching, 1999; Otte and Pleim,
2010) to generate model-ready meteorology for chemical transport simulations.

2.2.6 WRF-CHEM

The WRF/Chem-Hg model (Gencarelli et al., 2014; 2015; 2016) is a modified
version of WRF/Chem (version 3.4, Grell et al., 2005) model, developed to
350 reproduce the emission, transport, chemical transformation and deposition of Hg
at local scales with elevated spatial and temporal resolutions. The gas phase
chemistry of Hg and a parametrized representation of atmospheric Hg aqueous
chemistry have been added to the RADM2 chemical mechanism using KPP (Sandu
and Sander, 2006) and the WKC coupler (Salzmann and Lawrence, 2006), in order
355 to represent four Hg species: GEM, GOM, PBM, and dissolved oxidized mercury
($\text{Hg}^{\text{II}}_{(\text{aq})}$) (see Gencarelli et al., 2014 for further details regarding Hg
parametrizations and the physics options employed). Oxidation by O_3 , OH and Br
was implemented as described in Gencarelli et al., 2015, in accordance with the
experimental purpose. In the BASE case only O_3 and OH chemistry are used.
360 Chemical Initial and Boundary Conditions (IC/BC) were taken from the ECHMERIT
model (Jung et al., 2009; De Simone et al., 2014) for Hg species, while boundary
conditions for other chemical species were taken from MOZART-4 (Emmons et al.,
2010). Dry deposition of gas-phase species is treated using the approach
developed by Wesely (1989), multiplying the concentrations in the lowest model
365 layer by the spatially and temporally varying deposition velocity, which is
proportional to aerodynamic, sublayer, and surface resistances. The wet
deposition of Hg species has been implemented by adding the Hg compounds to
the scheme in WRF/Chem for gas and particulate convective transport and wet
deposition. In-cloud and below-cloud scavenging of Hg species have been treated
370 in accordance with the approach described by Neu and Prather (2012), with Hg



species scavenging rate assumed to be the same as that for $\text{HNO}_3(\text{g})$. The model domain covers Europe and the Mediterranean Sea, including part of the western North Atlantic Ocean, North Africa and the Middle East with a horizontal resolution of 24×24 km, and 30 vertical levels from soil to 50 hPa. Hg emissions by
375 AMAP/UNEP (2013a, 2013b) for mercury and from the EDGARv4.tox1 (2008) inventory for other species were interpolated on this model domain.

2.2.7 CCLM-CMAQ

This modelling system is based on the meteorological model CCLM and the
380 chemistry transport model CMAQ v5.0.1. All physical atmospheric parameters were taken from regional atmospheric simulations with the COSMO-CLM v4.8 mesoscale meteorological model (Geyer, 2014) using NCEP reanalysis data as forcing (Kalnay et al., 1996). COSMO-CLM is the climate version of the regional scale meteorological community model COSMO (Rockel et al., 2008), originally
385 developed by Deutscher Wetterdienst (DWD) (Steppeler et al., 2003; Schaettler et al. 2008). It has been run on a $0.22^\circ \times 0.22^\circ$ grid using 40 vertical layers up to 20 hPa for the whole of Europe. COSMO-CLM uses the TERRA-ML land surface model (Schrodin and Heise, 2001), a TKE closure scheme for the planetary boundary layer (Doms, 2011; Doms et al., 2011), cloud microphysics after Seifert and
390 Beheng (2001, 2006), the Tiedtke scheme (Tiedtke, 1989) for cumulus clouds and a long wave radiation scheme following Ritter and Geleyn (1992). The meteorological fields were then processed to match the Lambert Conformal Conical CMAQ grid with a grid size of 24×24 km with 30 sigma hybrid layers up to 50 hPa. CMAQ uses the information that is provided by the meteorological input
395 fields to calculate transport, transformation and loss of all gas phase and particulate species (Byun & Ching, 1999; Byun & Schere, 2006). For this study we used the multi-pollutant version with the carbon bond 5 photochemical mechanism cb05tump (Tanaka et al., 2003; Yarwood et al., 2005; Sarwar et al., 2007; Whitten et al., 2010) and the aerosol module aero6 (Appel et al., 2013;
400 Carlton et al., 2010; Foley et al., 2010). Deposition schemes are based on Byun and Schere (2006) for dry and Pleim and Ran (2011) for wet deposition. The



mercury chemistry is based on Bullock and Brehme (2002) and was updated based on observations and model inter-comparisons in the course of the EU FP7 project GMOS (Global Mercury Observation System) (Zhu et al., 2015; Bieser et al., 2014a, 2014b). To describe the re-emission of deposited mercury we used the bi-directional flux parametrization following Bash et al. (2010). Additionally, emissions from the North- and Baltic Sea were estimated based on Bieser and Schrum (2016). Boundary conditions were obtained from the GLEMOS model for GEM, GOM, PBM (Travnikov and Ilyin, 2009) and from TM-5 for all other species (Huijnen et al., 2010). The annual total emissions are based on AMAP for mercury (AMAP, 2013a, 2013b) and EMEP for other species and were speciated and disaggregated to an hourly resolution with the SMOKE for Europe emission model (Bieser et al., 2011a). Plume rise of point sources was explicitly calculated based on Bieser et al., (2011b). Finally biogenic emissions were calculated on-line using the BEIS3.14 model (Schwede et al., 2005; Vukovich et al., 2002).

2.3 Sensitivity runs

To evaluate the impact of emissions and atmospheric chemistry on the vertical distribution of mercury a set of sensitivity runs was made. While for the BASE case each model uses its default setup, for the sensitivity runs certain aspects of the models were harmonized. The list of all sensitivity runs is given in Table 2. Concerning emissions, we tested the impact of anthropogenic emissions by considering only natural and legacy emissions (NOANT) and by altering the speciation of anthropogenic emissions to 100% GEM (ANTSPEC). In addition, we investigated different oxidation reactions by considering only one reaction at a time, namely ozone (O3CHEM), hydroxy radicals (OHCHEM), and bromine (BRCHEM). In these cases, the models used the same input fields for the investigated reactant. For bromine chemistry two alternative sets of bromine fields were used from GEOS-Chem (BRCHEM1) and from the p-TOMCAT model (BRCHEM2).

2.4 Model evaluation



For the model evaluation the grid cell and time step matching each individual measurement were taken. This means for example that observations within a
435 single vertical profile can correspond to different time steps in the model. Due to the small amount of aircraft observations available, such a comparison faces the problem that the model bias will not average out as it tends to do for larger data sets (e.g. 8760 hourly observations for a single year of ground-based station data). Moreover, the vertical model performance is highly dependent on
440 meteorological parameters (e.g. PBL height, vertical transport). Thus, for an individual profile the model bias can be quite large. We did not perform a detailed analysis of the meteorological fields because it is beyond the scope of this paper. To increase sample sizes, we summed several vertical profiles into seasonal average profiles in order to increase the number of observations per altitude.
445 Moreover, to completely remove the model bias from the analysis of the vertical distribution of mercury we calculated a relative vertical profile which we call the mean deviation profile (MDP). The MDP indicates the difference for each individual altitude from the average column concentration and is calculated for models and observations independently. Thus, it indicates whether each model is able to
450 reproduce the observed vertical distribution rather than the actual concentration of mercury species (Eq-3). This is especially valuable for the analysis of oxidized mercury species, as there is an ongoing discussion about an underestimation of concentrations due to limitations of the current measurement techniques (Lyman et al., 2016; Ariya et al., 2015; Gustin et al., 2015; Huang and Gustin, 2015; Jaffe et al., 2014; McClure et al., 2014; Ambrose et al., 2013; Huang et al., 2013; Kos et al., 2013; Lyman et al., 2010) Such a systematical measurement error is canceled out in the calculation of the MDP (Eq. 3).

Individual Layer Mean $\bar{X}_L = \frac{1}{N} \sum_{L,i=1,N_L} X_{(i,L)}$ (Eq. 1)

460 Total Column Mean $\bar{X} = \frac{1}{M} \sum_{L=1,M} \bar{X}_L$ (Eq. 2)



Mean Deviation Profile $MDP_L = \frac{\bar{X}_L - \bar{X}}{\bar{X}}$ (Eq. 3)

$X_{(i,L)}$ model or observation i in layer L

L layer

N_L number of values in layer L

i counter for values in layer L

M number of layers in profile

465

3. Results and Discussion

Observations indicate that there is a tripartite distribution of total mercury (TM) in
470 the atmosphere. The highest concentrations (1.4 – 1.8 ng m⁻³) are found inside the
PBL with a strong gradient towards the free troposphere (1.1 – 1.4 ng m⁻³). This
gradient seems to be mainly driven by anthropogenic emissions, as it was not
observed in regions with low primary emissions (e.g. Mace Head, Ireland)
(Sprovieri et al., 2016; Weigelt et al., 2015). Finally, in the stratosphere total
475 mercury concentrations are typically below 1 ng m⁻³ (0.7 – 1.0 ng m⁻³) (Slemr et
al., 2016; Lyman and Jaffe et al., 2012). The observed TM profiles are often similar
to GEM profiles. Inside the PBL oxidized mercury (RM) (Here, RM is defined as the
sum of all oxidized forms of mercury including GOM and PBM)) concentrations are
very low and mostly between 20 – 100 pg m⁻³ in Europe and North America, even
480 in source regions (Sonke et al., 2016; Weigelt et al., 2016; 2013; Gay et al., 2013;
Torseth et al., 2012; Prestbo and Gay, 2009). CARIBIC measurements during
intercontinental flights indicate that RM concentrations are also usually below 100
pg m⁻³ in the upper free troposphere (9000 – 12 000m) and only occasionally do
high RM concentrations occur which are probably caused by the direct inflow of
485 RM from the stratosphere, or the inflow of oxidizing agents which then react with
GEM (Lyman and Jaffe, 2012). A combination of ETMEP and CARIBIC observations
over Germany resulted in a uniform TM and GEM distribution in the free
troposphere during summer (Weigelt et al. 2016) and TM concentrations close to
490 those measured at ground level were found on 6 overflights of the CARIBIC
aircraft in April, June, and September. A similar vertical distribution was found in



North America during winter (Brooks et al., 2014) and summer (Ambrose et al., 2015; Gratz et al., 2015; Shah et al., 2015). In none of these cases a substantial TM gradient was found inside the free troposphere and the GEM/TM ratio was in the range of 0.95 - 0.99 in the upper free troposphere which is a ratio typically found inside the PBL. During spring (14th April to 4th June) Brooks et al. (2014) consistently found low TM concentrations above 5000m which indicates a stratospheric intrusion of air masses with low mercury concentrations. Here, the GEM/TM ratio in the upper troposphere decreased to 0.88 to 0.92. For comparison, GEM/TM ratio at the tropopause is around 0.8 - 0.9 and decreases to 0.6-0.8 in the first 4 km above the tropopause. A similar profile was observed by Gratz et al. (2015) on the 24th June and could be attributed to high bromine concentrations. Bromine as the main oxidizing agent in the upper free troposphere is consistent with findings from CARIBIC that showed no consistent influence of ozone concentrations on the GEM/TGM ratio (Fig. S1).

Finally, in North America a peak of RM concentrations in the range of 100 - 300 pg m⁻³ with GEM/TM ratios below 0.9 was observed in the lower free troposphere (2000 - 4000m). As there are no airborne observations in the range of 3500 - 6500m this feature has not yet been observed over Europe. Possible reasons for the occurrence of this RM peak, which points to GOM production at this altitude, are still unclear. However, it may be speculated that low relative humidity, low particle surface density, and high solar radiation facilitate photochemistry above the PBL. Based on the findings above, Figure 1 depicts idealized seasonal vertical profiles for the northern mid-latitudes.

Here, we investigate capability of the models to reproduce the observed atmospheric distribution of TM, GEM, and RM. To increase the sample size for the model evaluation we created seasonal average profiles for Europe and North America. For this, we integrated the high resolution 2.5 minute Tekran data to hourly values, separated all observations into bins of 1000m (0 - 1000, 1000 - 2000, etc.) and calculated the mean concentration as well as the 66% quantile range for each bin. In addition to the absolute concentrations we investigate mean deviation profiles as described in Section 2.4.



3.1 Total and Elemental Mercury

525 3.1.1 Europe

Based on the combination of ground based observations from the GMOS network (Sprovieri et al., 2016; GMOS, 2016; Weigelt et al., 2013; 2015) and ETMEP observations inside the PBL and the lower troposphere (Weigelt et al., 2016), as well as CARIBIC observations in the upper troposphere and the lower stratosphere
530 (Slemr et al., 2016) we were able to obtain comprehensive vertical mercury profiles for Europe from the surface up to 12 000m. Here, we present two individual profiles (Figure 2):

The first profile measured on 21st August 11 - 12h UTC at Leipzig, Germany which combines ETMEP and CARIBIC data and was published by Weigelt et al. (2016).
535 Based on the discussion above and ETMEP GOM measurements being in the range of 20 to 40 pg m^{-3} we expect GEM to be almost identical to TM for these profiles, perhaps except for the data gap in the range of 3000 - 6000m where GOM concentrations could have been higher. It can be seen that the models generally underestimate mercury concentrations. This is in line with many previous model
540 studies which found that models tend to underestimate current TM concentrations in Europe (Bieser et al., 2014; Chen et al., 2014; Muntean et al., 2014; Gencarelli et al., 2016). However, the majority of model values are still within the measurement uncertainty range (Fig. 2). Looking at the vertical distribution we found that the models are generally able to reproduce the vertical distribution of
545 both GEM and TGM. However, the PBL height as calculated by the meteorological models has a large influence on the actual altitude of the Hg gradient. It can be seen, for example, that WRF-Chem simulates a PBL height of 500m, while the observations located the top of the PBL at an altitude of 2500m. Here, the PBL growth was delayed in the WRF meteorological model. All models exhibit higher
550 concentrations inside the PBL and none has a gradient inside the troposphere, which is in agreement with the observations. Concerning the GEM/TGM ratio only one model show values lower than 0.9 - 0.95 inside the troposphere. The



ECHMERIT model exhibits a mostly uniform GEM/TGM ratio between 0.7 and 0.8 over the whole altitude range. This would be a realistic ratio if RM measurements
555 were underestimated by a factor of 5.

Looking at the stratosphere, only the GLEMOS model is able to reproduce a decrease of TM concentrations above the tropopause. Due to the low resolution in this altitude, GLEMOS has only 2 layers between 10 000 and 15 000m, the modeled gradient is less steep than that observed. None of the other models
560 gives significantly lower TM concentrations in the stratosphere. However, GEOS-Chem and GEM-MACH-Hg have increased oxidation above the tropopause. In GEM-MACH-Hg the GEM/TM ratio declines from 0.9 at the tropopause (11 000m) to 0.6 5km above. This is in line with observations from CARIBIC. The GEOS-Chem model also exhibits pronounced mercury oxidation above the tropopause with the
565 GEM/TM ratio declining from 0.9 to 0.1 in the 5km above the tropopause. ECHMERIT and WRF-Chem-Hg have no increased oxidation or reduced TM concentrations above the tropopause. The CMAQ-based models CCLM-CMAQ and CMAQ-Hem have the tropopause as their upper boundary and do not model the stratosphere.

570 The second profile is a combination of ground based observations at the GMOS station Mace Head, Ireland with the CARIBIC flight of 19th September 6 - 7 - 8h UTC (Fig. 2). In 2013, the CARIBIC aircraft passed close to Mace Head six times within a range of 86 - 220km (27th April, 28th April, 08th June, 07th June, 19th September, 20th September) but the other profiles look similar. The CARIBIC data
575 is separated into tropospheric and stratospheric measurements based on the relative height above the tropopause (Sprung and Zahn, 2010). Here, we depict the profile for the nearest CARIBIC overflight. In this region, which is influenced by clean air from the Atlantic Ocean, we did not observe a gradient between the surface and the upper troposphere. Again, models tend to underestimate mercury
580 concentrations. At Mace Head all models are able to reproduce the linear TM concentrations in the free troposphere. However, several models overestimate the concentrations near the surface. It has to be noted, however, that Mace Head is a coastal station with predominantly westerly winds from the open Atlantic which



might be difficult to reproduce for models with a coarse resolution and thus higher
585 ground based concentrations could be due to anthropogenic emissions from
Ireland. At the tropopause, the observations show an almost instantaneous
decrease of TM concentrations from 1.4 to 1.0 ng m⁻³. The models behave
similarly to the profile over Leipzig with only GLEMOS showing a decrease above
the tropopause. The models with a higher vertical resolution near the tropopause
590 (GEM-MACH-Hg 12 layer and GEOS-Chem 5 layers between 10 000 and 15 000m)
are better able to reproduce the gradient, albeit they only show a decrease in
GEM/TM ratio not in TM concentration.

As described above we calculated an average summer vertical profile for Europe
using data from 5 ETMEP profiles in Germany and Slovenia performed between
595 the 19th and 23rd August complemented with CARIBIC flights on the 21st and 22nd
August and the 18th and 19th September. Thus, we created an average profile with
290 hourly samples based on a sampling interval of the co-located Tekran
instruments of 2.5 minutes (Fig. 4). We did not use measurements from the Lumex
instrument for this evaluation as none of the other aircraft were equipped with
600 such an instrument. The performance of the Lumex instrument on this flight is
discussed in Weigelt et al. (2016, this issue). The resulting GEM and TM profiles
are depicted in Figure 3a and 3b respectively. Again, it can be seen that the
models generally underestimate mercury concentrations in central Europe during
August 2013. However, when looking at the mean deviation profile (MDP) which
605 depicts the relative vertical distribution compared to the total column average
concentration, all the models are within the observed range. Investigating the
experimental model runs, it can be seen that in the case with all anthropogenic
emissions emitted as elemental mercury (ANTSPEC) the models have slightly
higher mercury concentrations near the surface which leads to better agreement
610 with observed gradients. While all models give similar vertical profiles for the
BASE and ANTSPEC cases, in the cases without anthropogenic emissions (NOANT)
and without atmospheric chemistry (NOCHEM) the models show different
responses. In these cases the modeled vertical distributions of mercury start to
diverge from the observations and each other. This shows the strong impact of



615 atmospheric chemistry on the vertical GEM distribution and global mercury
transport in general.

3.1.2 North America

We created similar average vertical mercury profiles for North America based on
620 185 hourly samples from three profile flights at Tullahoma, TN between 18th
January 2013 and 14th June 2013 (Brooks et al., 2014) (Figure 4) and 898 hourly
samples from 7 NOMADSS flights between 20th June 2013 and 12th July 2013
(Figure 5). For the NOMADSS flights we selected vertical flight paths for this
evaluation and discarded horizontal flight paths. Here, the observations exhibit a
625 similar vertical distribution with higher concentrations inside the PBL and lower
concentrations in the FT. The NOMADSS profile contains one flight with a
stratospheric intrusion and thus shows a slightly decreasing trend in the upper
troposphere. Observed profiles and model results for North America are
comparable to Europe. For the summer profile (Fig. 5) there are elevated TM
630 concentrations inside the PBL and no trend inside the FT. Models tend to
underestimate TM and GEM concentrations but are in good agreement with the
relative distribution. The higher concentrations near the surface in the ANTSPEC
case leads to better agreement with observations. For the winter profile (Fig. 4)
GEOS-Chem and GEM-MACH-Hg are in good agreement with the absolute GEM
635 and TM observations. However, models do overestimate concentrations near the
surface, which could be due to modelled PBL height and anthropogenic emission
fluxes.

Finally, we created a third profile for spring from three profile flights at Tullahoma,
TN on 15th April, 10th May, and 4th June 2013 (Brooks et al., 2014) (Figure 6). This
640 profile looks different than the others. Again, TM and GEM concentrations are
highest inside the PBL but there is a second decreasing gradient between 4000
and 5000m. Above 6000m GEM and TM concentrations fall below 1.0 ng m^{-3} which
is a value typically found in the stratosphere. This feature was observed on all
three flights during spring and thus seems not to be an individual outlier.
645 Furthermore, in the time from April to July stratospheric mass transport into the



upper and mid troposphere is known to occur regularly (Appenzeller and Holten, 1996; Allen et al., 2003; Zanis et al., 2003; Olsen et al., 2004; Schoeberl 2004). Moreover, Sprenger et al. (2003) and Sprenger and Wernli (2003) demonstrated that cross tropopause mass flux is highest in the mid latitudes where these
650 mercury profiles were measured. This is also in line with observations from CARIBIC which found stratospheric intrusions of air masses with low mercury concentrations during this time span (Slemr. p.c.). Stratosphere to troposphere transport of mercury is also the most convincing reason for observed elevated oxidized mercury concentrations in the upper troposphere which is further
655 discussed in the next Section.

3.2 Oxidized mercury

Apart from GEM no individual mercury compound has been identified so far. The speciation of mercury is thus operationally defined as GEM, GOM, and PBM (Gustin
660 et al., 2015). As the different implementations of the mercury red-ox chemistry in the models presented here is not directly compatible, we decided to sum all oxidized model species for this comparison. Thus, in the following Section we compare modeled reactive mercury RM ($RM = GOM + PBM = TM - GEM$) concentrations to observations mostly because of the supposed equilibrium
665 between GOM and GEM (Rutter and Schauer, 2007; Amos et al., 2012). The species measured by the presented aircraft campaigns also differ. Some measure GOM and PBM explicitly and others measure the difference between TM and GEM. Moreover, depending on the sampling inlet geometry and operating conditions, filters in the sampling line, and temperature gradients, a fraction of PBM may not
670 be accessible to measurement (Slemr et al., 2016). In the following we treat all observations alike and interpret them as total RM measurements.

3.2.1 Europe

Measurements at Waldhof, Germany indicate that there is a strong RM gradient
675 inside the PBL with very low concentrations at the surface and 10 - 15 times higher concentrations above 500m. This is to be expected because of the high



stickiness and therefore fast dry deposition of RM on surfaces (Zhang et al., 2009). During the ETMEP campaign a total column RM measurement was performed inside the PBL above the ground based measurement station Waldhof (Figure 6). Five of the seven models are able to reproduce the RM concentrations above the surface with one over and one underestimating the concentration. It has to be noted, that ECHMERIT which strongly overestimates RM is able to reproduce the low concentrations at the surface and thus is in good agreement with the relative vertical distribution. An investigation of the experimental model runs indicated that the overestimation at the surface is due to anthropogenic emissions and was reduced significantly in the ANTSPEC run while concentrations above the surface are mainly driven by atmospheric chemistry. This is in line with the findings of Bieser et al. (2015) and Weigelt et al. (2016).

3.2.2 North America

For North America, we use the same profiles as described in Section 3.1.2. On the flights at Tullahoma GOM as well as PBM was measured and for the analysis we plotted the sum as total RM. Due to the long sampling times necessary for denuder measurements the sample size is much smaller than for the GEM observations. The winter profiles are based on 32 samples (Fig. 7) and the spring profiles on 48 samples (Fig. 8).

During winter, RM concentrations varied around 30 pg m^{-3} with slightly lower concentrations inside the PBL. For the BASE case model results are mostly inside the uncertainty range of the observations. During winter the models with the lowest RM production (GEM-MACH-Hg, GLEMOS, CMAQ-Hem) are closest to the observations. ECHMERIT generally overestimates RM concentrations, while GEOS-Chem provides increasing concentrations above 4000m which are not in agreement with observations. This increasing trend was also found in models when using the GEOS-Chem and p-TOMCAT bromine fields (BRCHEM1 and BRCHEM2). However, the peak is much more pronounced in the GEOS-Chem run. Further investigation of the experimental model runs indicates that the amount of oxidized mercury is strongly dependent on the choice of CTM. For example, the



ECHMERIT model produces the highest RM concentrations for all chemical reactions. With the exception of ECHMERIT all models are closest to the observations in the BASE case. Looking at the relative vertical distribution, the observations give lower RM concentrations inside the PBL and no trend in the free troposphere. The gradient at the PBL can be reproduced by all chemical reactants but bromine and OH chemistry leads to an increasing trend in the upper troposphere (Fig. 8). Here, only the ozone chemistry is able to reproduce the observed profiles.

The spring profile for RM at Tullahoma is depicted in Figure 9. Here, a strong RM peak up to 150 pg/m³ can be seen in an altitude of 3000 - 5000m. This peak is above the PBL which was between 2500 and 3200m during these flights which were all made during the afternoon when the PBL reaches its highest expansion. In the BASE case most models fail to reproduce this peak and only CMAQ-Hem and ECHMERIT, both using ozone chemistry, give similar vertical profiles. On average, the multi-model mean is close to the observed concentrations, but exhibits only the typical gradient at the PBL but no pronounced RM peak. Investigating the relative vertical distribution for different chemistry sensitivity runs reveals that ozone and OH chemistry are able to reproduce the observed peak. For bromine chemistry the profiles are inverted, exhibiting a minimum where the maximum RM concentrations were observed. Comparing the RM profiles to the TM profiles (Fig. 6) shows that the RM peak is below the presumably stratospheric low TM air masses. This could be an indication that the increased oxidation is not due to stratospheric bromine transport but due to regional oxidation above the PBL. This would explain, why the bromine chemistry cannot reproduce this peak but ozone and OH chemistry can. Of course it has to be stated that the bromine fields themselves are also subject to large uncertainties and thus the interpretation of these findings depends on the quality of the bromine fields. However, results are similar for independent bromine datasets from GEOS-Chem and p-TOMCAT bromine fields. Furthermore, there were only two RM measurements which indicate the decline above 6000m and it would also be possible that this peak extended further upwards and was due to a deep



stratospheric intrusion.

740 Finally, we evaluate the model performance for RM for the summer profile based
on NOMADSS data from June and July 2013. Due to the differential measurements
approach of the DOHGS instrumental setup the sample size is equal to that of the
GEM profiles (Lymann and Jaffe, 2012; Ambrose et al., 2013; Ambrose et al. 2015).
The larger sampling size together with the fact that NOMADSS observations cover
745 a region larger than the vertical profiles over Tullahoma leads to a higher
variability in the measurements given by the 66% quantile range (Fig. 10). We
created the average RM profile from the same data as the GEM profile. For RM
measurements below the detection limit we used half the reported detection limit
which varied between 74 and 138 pg m^{-3} . Thus, giving us a minimum RM
750 concentration of 34 pg m^{-3} which is in line with the other observations previously
presented.

The resulting profile exhibits a distinct vertical distribution with lower
concentrations inside the PBL (40 – 60 pg m^{-3}), an RM peak directly above the PBL
(100 – 350 pg m^{-3}), lower concentrations in the mid-troposphere (50 – 200 pg/m^3),
755 and increasing concentrations in the upper troposphere (100 – 300 pg/m^3). The
increasing trend in the upper troposphere was attributed to an episode with high
bromine concentrations (Gratz et al., 2015) and accordingly the model runs with
bromine chemistry can reproduce this (Fig. 10, BRCHEM). The finding that the
ozone and OH reactions cannot reproduce the observed increase in RM
760 concentrations in the upper troposphere is in line with findings from CARIBIC,
where no correlation of ozone with the GEM/TM ratio found (Fig. S1).

Similarly to the spring profile at Tullahoma, the lower RM peak lies directly above
the PBL, which is an area of enhanced photolytic activity due to higher solar
radiation and low particle density concentrations compared to the PBL. Also, due
765 to the low water vapor content in this region little aqueous reduction of RM can
take place. This RM peak cannot be reproduced by model runs with bromine
chemistry. In fact, the resulting profiles are even inverse to the observations.
Ozone and OH chemistry on the other hand, lead to increased oxidation above the
PBL with the OH chemistry run having the best agreement with the observed



770 vertical distribution and ozone with the actual concentrations (Fig. 10, O3CHEM,
OHCHEM).

3.2.3 Stratosphere

775 Stratospheric observations from inter-continental CARIBIC flights indicate that the
GEM/TM ratio declines above the tropopause with values typically in the range
between 0.6 and 0.8 in the first 4km above the tropopause (Fig. 11). During
summer values down to 0.5 were found in the tropics. Here, we compare those
models which include the stratosphere (GLEMOS, GEM-MACH-Hg, GEOS-Chem,
ECHMERIT) to observations. The models exhibit greater differences in the
780 stratosphere compared to the troposphere. ECHMERIT exhibits no GEM/TM
gradient throughout the year with similar values of 0.7 - 0.9 in troposphere and
stratosphere. Although the model cannot reproduce the declining trend above the
tropopause, it is mostly within the uncertainty range of the observations.

785 GLEMOS shows the best agreement with observations. It is able to reproduce the
slow GEM/TM ratio decrease above the tropopause with values mostly between
0.5 and 0.7 in the first 4km above the tropopause. GEM-MACH-Hg and GEOS-
Chem both exhibit much higher oxidation rates in the stratosphere. GEM-MACH-Hg
also has a slow decrease of GEM/TM ratios above the tropopause but consistently
790 shows GEM/TM ratios below 0.3 above 12 000m north and south of 30°. Finally, in
GOES-Chem the GEM/TM ratio decreases earlier, already a few kilometers below
the tropopause in altitudes of 6000 - 10 000m. Above 12 000m almost all mercury
is oxidized at the poles and even at the equator the GEM/TM ratio drops below 0.1
above 16 000m (Fig. 11c). On flights during summer in the range of 30°N - 0°N
795 a steep decline of the GEM/TM ratio to values below 0.5 was observed, which is in
line with the profiles modeled by GEOS-Chem. However, it has to be considered
that the uncertainty of the observations is high and at times no gradient at all was
observed. The GEM and TM CARIBIC measurements are further discussed in
Section 3.3.

800



3.3 Inter-hemispheric gradients

Finally, observations on 8 flights from Munich, Germany to Cape Town, South Africa and 19 flights from Munich to Sao Paulo, Brazil are used to investigate the models' capability to reproduce inter-hemispheric gradients. The inter-hemispheric CARIBIC flights were performed between 2013 and 2017. The CARIBIC Tekran instrument, which is usually set up to measure TM, was equipped with a quartz wool filter on each return flight to measure GEM only (Slemr et al., 2016). The Tekran raw data was manually reintegrated (Slemr et al., 2016). This allows us to look at inter-hemispheric gradients of elemental and total mercury.

805 However, as the two quantities were not measured on the same flights only a range of possible oxidized mercury concentrations can be deduced. Long range transport and a variable tropopause height can easily lead to differences larger than the expected RM concentrations on the return flight on the same flight track. Because of this, the calculated average difference of TM and GEM can sometimes

815 be lower than zero. Most of the TM and GEM measurements were within each other's 66% quantile range (Fig. 12a,b). The difference between the average TM and GEM concentrations was 70 pg m^{-3} on the flights to Cape Town (N=756) and 100 pg/m^3 on the flights to Sao Paulo (N=1399). A detailed investigation leads to the conclusion that RM concentrations are mostly low ($\sim 50 \text{ pg m}^{-3}$) in the upper

820 troposphere with occasionally high concentrations of up to 200 pg m^{-3} and more. This is in line with the findings presented in Section 3.2, and with three of the four global models which also give an average TM - GEM difference of around 100 pg m^{-3} . GLEMOS, GEM-MACH-Hg, and ECHMERIT are in good agreement with observations in the BASE case while GEOS-Chem overestimates oxidized mercury

825 in the mid latitudes ($50^\circ\text{N} - 30^\circ\text{N}$), leading to an average of 200 pg m^{-3} (Fig. 12c,d). The results for the sensitivity runs using different chemical reactants leads to similar results and the other models also exhibit increased oxidation in both bromine chemistry runs (Fig. 12g,h).

To create average inter-hemispheric transects we grouped all observations which

830 were at least 1 km below the tropopause into bins of 5° latitude and filtered out high mercury concentrations from polluted air masses ($\text{Hg} > 2.5 \text{ ng/m}^3$). This was



especially necessary on the flights to South Africa where a few large scale biomass burning events lead to measured GEM concentrations of up to 3 ng m^{-3} . These events can mask the inter-hemispheric gradient. Finally, the first and last
835 data points include take-off and landing. This results in a stronger gradient compared to measurements in the upper troposphere.

For the model evaluation we use monthly average GEM and TM concentrations for the month during which each flight was performed from the grid cell closest to the aircraft and aggregate the model data into bins similar to the observational data.

840 It has to be kept in mind that for models with a low vertical resolution the relevant grid cell might extend above the tropopause. Here, we focus on the relative inter-hemispheric gradient to evaluate the models. The relative TM and GEM trends on flights to Sao Paulo are depicted in Figure 13 and absolute values are given in Figure 14. Similar plots for the flights to Cape Town are given in the
845 supplementary material (Figures S2 and S3). The models are generally in better agreement with absolute and relative observations for total mercury (Fig. 13, 14). This is mainly due to an overestimation of oxidized mercury in the northern hemisphere (45°N to 35°N). All models give slightly better results in the ANTSPEC case and the absolute mercury concentrations are 10% higher compared to the
850 BASE case (Fig. 14c,d). This is consistent with the findings in Section 3.1. In the case without anthropogenic emissions (NOANT) mercury concentrations are much too low and in the NOCHEM run models vastly overestimate mercury concentrations. This is to be expected, as the lifetime of GEM increases without oxidation processes. The exception is the ECHMERIT model which is very close to
855 observations in the NOCHEM case. This is due to the fact that the ECHMERIT model does not consider dry deposition of GEM. The results in all experimental chemistry runs are strongly dependent on the dynamic response of air-sea exchange. In models that prescribe fixed oceanic emission rates, changing deposition due to changes in the chemistry scheme, cannot be compensated by
860 re-emissions. The ECHMERIT model for example prescribes fixed oceanic mercury concentrations and thus an increase in deposition will result in lower TM concentrations and vice versa, which explains the very high TM concentrations in



chemistry sensitivity runs. This underlines the importance of the air-sea exchange for global atmospheric models even near the tropopause.

865 For TM, no chemistry setup could be found that most accurately reproduced the observed concentrations and trends. As was shown before in the evaluation of the vertical profiles, differences in the CTM formulation can have a larger impact than the choice of oxidant. Looking at GEM, it can be seen that different oxidants lead to different inter-hemispheric distributions. Here, the use of bromine fields leads to
870 an overestimation of oxidation in the northern hemisphere (50°N - 25N). On the other hand, the use of ozone and OH chemistry only leads to underestimation of the oxidation around the equator. However, the GEM-MACH-Hg model does not exhibit this feature. With 12 layers between 10 000 and 15 000m the GEM-MACH-Hg model has a much greater vertical resolution around the tropopause compared
875 to the other models and this has a large impact on model results. In models with coarser vertical resolution, low stratospheric concentrations will have a larger impact on this evaluation. GLEMOS and ECHMERIT are the models with the lowest resolution in this altitude with 2 and 3 layers between 10 000 and 15 000m respectively. GEOS-Chem has 5 layers in this altitude.

880

4. Conclusions

In this model inter-comparison study we investigated the vertical distribution of mercury in the atmosphere and evaluated the impact of mercury chemistry and emissions. The key finding is that models are generally able to reproduce the
885 vertical profile of total mercury (TM) and elemental gaseous mercury (GEM) from the surface up to the tropopause. This means largely uniform concentrations inside the PBL and free troposphere. Increased GEM concentrations observed inside the PBL could be attributed to anthropogenic emissions. However, the models tend to overestimate GEM concentrations in the lower stratosphere and
890 those models which feature declining GEM concentrations above the tropopause do so by oxidation to reactive mercury (RM) species, thus overestimating TM. Moreover, it was found that a high vertical resolution near the tropopause is very important for a better reproduction of the observed declining mercury gradient.



895 The RM, the observations indicate low concentrations inside the PBL, often below
50 pg m^{-3} with a strong decrease towards the surface. This seems plausible due to
the high dry deposition velocity of RM. Current model setups tend to overestimate
RM near the surface which here could be attributed to the current speciation
profiles used for anthropogenic emissions. Also in the FT, most observations are
900 below 100 pg m^{-3} which is approximately the detection limit of current
measurement techniques. Therefore, no further information on possible vertical
gradients is available for these regions. However, two separate regions in the
upper and lower free troposphere with increased GEM oxidation and RM
concentrations above 100 pg m^{-3} up to 500 pg m^{-3} were identified in North
905 America independently by Brooks et al. (2014) and Ambrose et al. (2013).
Because current measurement techniques have been shown to underestimate
concentrations of oxidized mercury (Jaffe et al., 2014; Gustin et al., 2015), we
have focused the model evaluation on relative vertical distributions which are not
subject to systematical measurement errors.

910 Our interpretation of the observations is that stratospheric intrusions and
tropopause folds, which mainly occur during spring time, play an import role for
elevated RM concentrations in the upper FT at altitudes above 6000m. The
frequency of stratosphere to troposphere transport is regionally variable and has
shown to be most common in the latitudes where the measurements were
915 performed. Supported by the observations of Gratz et al. (2015) the models imply
that bromine reactions are responsible for the oxidation of GEM during these
episodes. Besides bromine species, stratosphere to troposphere transport could
also be a source for RM already formed in the lower stratosphere. This would also
explain the missing correlation of ozone concentrations and GEM/TM ratios
920 measured by the CARIBIC aircraft in the upper FT.

Uniformly low RM concentrations were observed during winter and could be
reproduced by the models. In spring and summer, increased RM concentrations
were observed above the PBL in the lower free troposphere were observed during



925 spring and summer. This could only be reproduced by models using O₃ and OH
chemistry. Any oxidant directly above the PBL is either produced locally or
transported from the PBL and thus OH seems a plausible explanation. Moreover,
reduced water vapor content and particle surface densities would reduce any
occurring aqueous RM reduction processes.

930

Finally, we have investigated TM and GEM concentrations and gradients in the
upper troposphere between the northern and southern hemisphere based on
inter-continental CARIBIC flights. The models were more adept in reproducing TM
concentrations and trends compared to GEM. Model runs using bromine reactions
935 showed a better agreement to observed inter-continental TM gradients. However,
the current bromine fields lead to a strong overestimation of mercury oxidation in
mid-latitudes. Ozone and OH chemistry, on the other hand, led to overestimated
oxidation in the tropics. Interestingly, reducing the RM fraction in the
anthropogenic emission inventories led to a better agreement with observed
940 concentrations. This could be due high RM fractions for coal fired power plants in
current emission inventories which have high stacks and thus effective emission
heights can even be above the PBL at times.

List of contributors:

945 Modelling:

GLEMOS: Oleg Travnikov

GEOS-CHEM: Noelle Selin, Shaojie Song

GEM-MACH: Ashu Dastoor, Andrei Ryskov

ECHMERIT: Francesco De Simone, Ian Hedgecock

950 CMAQ-Hem: Che-Jen Lin, Yun Zhu

WRF-CHEM: Christian Gencarelli, Ian Hedgecock

CCLM-CMAQ: Johannes Bieser, Volker Matthias, Beate Geyer

p-TOMCAT: Xin Yang

955 Observations:

ETMEP: Andreas Weigelt, Johannes Bieser, Ralf Ebinghaus, Nicola Pirrone

NOMADSS: Daniel Jaffe, Jesse Ambrose, Lynne Gratz



Tulahoma: Steve Brooks, Xinrong Ren, Winston Luke, Paul Kelley

CARIBIC: Carl Brenninkmeijer, Andreas Zahn, Franz Slemr, Andreas Weigelt, Ralf Ebinghaus

960 Waldhof: Andreas Weigelt, Ralf Ebinghaus

Mace Head: Andreas Weigelt, Ralf Ebinghaus, Nicola Pirrone

References

- Allen, D.J., Dibb, J.E., Ridley, B., Pickering, K.E., Talbot, R.W. 2003. An estimate of the stratospheric contribution to springtime tropospheric ozone maxima using TOPSE measurements and beryllium-7 simulations. *JOURNAL OF GEOPHYSICAL RESEARCH*, VOL. 108, NO. D4, 8355, doi:10.1029/2001JD001428, 2003
- 965 AMAP/UNEP, Technical Background Report for the Global Mercury Assessment 2013a. Arctic Monitoring and Assessment Programme, Oslo, Norway / UNEP Chemicals Branch, Geneva, Switzerland. vi + 263 pp., 2013, available at <http://www.unep.org/chemicalsandwaste/Mercury/ReportsandPublications/tabid/3593/Default.aspx>, access: 1 November 2016.
- 970 AMAP/UNEP, Geospatially distributed mercury emissions dataset 2010v1, 2013b, <http://www.amap.no/mercury-emissions>, access: 1 November 2016.
- Ambrose, J.L., Lyman, S.N., Huang, J., Gustin, M.S., and Jaffe, D.A., 2013. Fast time resolution oxidized mercury measurements during the Reno Atmospheric Mercury Intercomparison Experiment (RAMIX). *Environmental Science & Technology* 47, 7285–7294, doi: 10.1021/es303916v
- 975 Ambrose, J.L., Gratz, L.E., Jaffe, D.A., Campos, T., Flocke, F.M., Knapp, D.J., Stechman, D.M., Stell, M., Weinheimer, A., Cantrell, C., and Mauldin, R.L., 2015. Mercury emission ratios from coal-fired power plants in the Southeastern United States during NOMADSS. *Environmental Science & Technology* 49, 10389–10387, doi: 10.1021/acs.est.5b01755.
- 980 Amos, H. M., Jacob, D. J., Holmes, C. D., Fisher, J. A., Wang, Q., Yantosca, R. M., Corbitt, E. S., Galarneau, E., Rutter, A. P., Gustin, M. S., Steffen, A., Schauer, J. J., Graydon, J. A., St Louis, V. L., Talbot, R. W., Edgerton, E. S., Zhang, Y., and Sunderland, E. M.: Gas-particle partitioning of atmospheric Hg(II) and its effect on global mercury deposition, *Atmos. Chem. Phys.*, 12, 591-603, doi:10.5194/acp-12-591-2012, 2012.
- 985 Amos, H.M., Sonke, J., H.M., Mason, R.P., Witt, M., Hedgecock, I., Corbitt, E.S., Sunderland, E.M. 2015. Observational and Modeling Constraints on Global Anthropogenic Enrichment of Mercury. *Environ. Sci. Technol.* 49, 4036-4047. doi: 10.1021/es5058665
- Appel, K.W., Pouliot, G.A., Simon, H., Sarwar, G., Pye, H.O.T., Napelnok, S.L., Akthar, F., Roselle, S.J., 2013. Evaluation of dust and trace metal estimates from the Community Multiscale Air Quality (CMAQ) model version 5.0.
- 990 Appenzeller, C. and Holton, J.R.. 2016. Seasonal variation of mass transport across the tropopause. *JOURNAL OF GEOPHYSICAL RESEARCH*, VOL. 101, NO. D10, PAGES 15,071-15,078, JUNE 27, 1996. Ariya PA, Amyot M, Dastoor A, Deeds D, Feinberg A, et al. 2015. Mercury physicochemical and biogeochemical transformation in the atmosphere and at atmospheric interfaces: A review and future directions. *Chem Rev* 115(10): 3760-3802. doi: 10.1021/cr500667e.
- 995 Balabanov, N., Shepler, B., Peterson, K.: Accurate global potential energy surface and reaction dynamics for the ground state of HgBr₂. *J. Phys. Chem. A*, 109, 8765-8773, 2005.
- Bergan, T., Gallardo, L., Rodhe, H. 1999. Mercury in the global troposphere: a three dimensional model study. *Atmos. Environ.* 33:1575-1585. doi: 10.1016/S1352-2310(98)00370-7
- 1000 Bey, I., Jacob, D. J., Yantosca, R. M., Logan, J. A., Field, B. D., Fiore, A. M., Li, Q., Liu, H. Y., Mickley, L. J., and Schultz, M. G.: Global modeling of tropospheric chemistry with assimilated meteorology: Model description and evaluation, *J. Geophys. Res.-Atmos.*, 106, 23073-23095, doi:10.1029/2001jd000807, 2001.
- Bieser J, Aulinger A, Matthias V, Quante M, Builtjes P. 2011a. SMOKE for Europe – adaptation, modification and evaluation of a comprehensive emission model for Europe. *Geosci Model Dev* 4: 47–68. doi: 10.5194/gmd-4-47-2011.
- 1005



- Bieser J, Aulinger A, Matthias V, Quante M, Denier van der Gon HAC. 2011b. Vertical emission profiles for Europe based on plume rise calculations. *Environ Pollut* 159: 2935–2946. doi: 10.1016/j.envpol.2011.04.030
- 1010 Bieser, J., De Simone, F., Gencarelli, C.N., Hedgecock, I.M., Matthias, V., Travnikov, O., Weigelt, A., A diagnostic evaluation of modeled mercury wet deposition in Europe using atmospheric speciated high-resolution observations, *Environ. Science and Pollution Research* 21 (16) 2014a.
- Bieser, J., Matthias, V., Aulinger, A., Geyer, B., Hedgecock, I.M., De Simone, F., Gencarelli, C.N., Travnikov, O. 2014b. Impact of Mercury Chemistry on Regional Concentration and Deposition Patterns. In: *Air Pollution Modeling and its Application XXIII* Eds. Steyn, D. and Mathur, pp 189-195, Springer. ISBN: 978-3-319-04378-4 R.
- 1015 Bieser, J. and Schrum, C., Impact of marine mercury cycling on coastal atmospheric mercury concentrations in the North- and Baltic Sea region. *Elementa* 111, 2016. doi: 10.12952/journal.elementa.000111.
- Bullock OR, Brehme KA. 2002. Atmospheric mercury simulations using the CMAQ model: Formulation description and analysis of wet deposition results. *Atmos Environ* 36: 2135–2146.
- 1020 Bullock, R.O., Atkinson, D., Braverman, T., Civerolo, K., Dastoor, A., Davignon, D., Ku, J.-Y., Lohman, K., Myers, T.C., Park, R.J., Seigneur, C., Selin, N.E., Sistla, G., Vijayaraghavan K. 2008. *JOURNAL OF GEOPHYSICAL RESEARCH*, VOL. 113, D17310. doi:10.1029/2008JD009803
- Byun DW, Ching JKS. 1999. Science Algorithms of the EPA Models-3 Community Multi-scale Air Quality (CMAQ) Modeling System. EPA/600/R-99/030. US EPA National Exposure Research Laboratory. Research Triangle Park, NC.
- 1025 Byun DW, Schere KL. 2006. Review of the governing equations, computational algorithms, and other components of the Models-3 Community Multiscale Air Quality (CMAQ) modeling system. *Applied Mechanics Reviews* 59(2): 51–77. 147–164. doi: 10.5194/essd-6-147-2014
- Brooks, S., Xinrong, R., Cohen, M., Luke, W.T., Kelley, P., Artz, R., Hynes, A., Landing, W., Martos, B. 2014. Airborne Vertical Profiling of Mercury Speciation near Tullahoma, TN, USA. *Atmosphere* 2014, 5(3), 557-574. doi:10.3390/atmos5030557
- 1030 Carlton, A.G., Bhave, P.V., Napelenok, S.L., Edney, E.O., Sarwar, G., Pinder, R.W., Pouliot, G.A., Houyoux, M., 2010. Model Representation of Secondary Organic Aerosol in CMAQv4.7. *Environmental Science and Technology*. 44 (22) 8553-8560.
- Chen, L., H.H. Wang, J.F. Liu, Y.D. Tong, L.B. Ou, W. Zhang, D. Hu, C. Chen and X.J. Wang, 2014. Intercontinental transport and deposition patterns of atmospheric mercury from anthropogenic emissions. *Atmos. Chem. Phys.*, 14:10163-10176.
- 1035 Cohen, M.D., Draxler, R.R., Artz, R.S., Blanchard, P., Gustin, M.S., Young-Ji, H., Holsen, T.M., Jaffe, D.A., et al., 2016. Modeling the global atmospheric transport and deposition of mercury to the Great Lakes. *Elementa: Science of the Anthropocene* 4 (000118), doi: 10.12952/journal.elementa.000118.
- 1040 Byun DW, Ching JKS. 1999. Science Algorithms of the EPA Models-3 Community Multi-scale Air Quality (CMAQ) Modeling System. EPA/600/R-99/030. US EPA National Exposure Research Laboratory. Research Triangle Park, NC.
- Byun DW, Schere KL. 2006. Review of the governing equations, computational algorithms, and other components of the Models-3 Community Multiscale Air Quality (CMAQ) modeling system. *Applied Mechanics Reviews* 59(2): 51–77. 147–164. doi: 10.5194/essd-6-147-2014/journal.elementa.000118.
- 1045 Dastoor, A., Larocque, Y. 2004. Global circulation of atmospheric mercury: a modelling study. *Atmospheric Environment* 38 (1) 147–161.
- Dastoor, A., Davignon, P., Theys, N., Van Roozendaal, M. Steffen, A., Ariya, P.A. 2008. Modeling dynByun DW, Ching JKS. 1999. Science Algorithms of the EPA Models-3 Community Multi-scale Air Quality (CMAQ) Modeling System. EPA/600/R-99/030. US EPA National Exposure Research Laboratory. Research Triangle Park, NC.
- 1050 Dastoor, A., Ryzhkov, A., Durnford, D., Lehnerr, I., Steffen, A., and Morrison, H.: Atmospheric mercury in the Canadian Arctic. Part II: Insight from modeling, *Sci. Total Environ.*, 509-510, 16-27, doi: 10.1016/j.scitotenv.2014.10.112, 2015.
- 1055 De Simone, F., Gencarelli, C.N., Hedgecock, I.M., Pirrone, N. 2014. Global atmospheric cycle of mercury: a model study on the impact of oxidation mechanisms. *Environmental Science and Pollution Research* 21 (6) 4110–4123.



- De Simone, F., Gencarelli, C. N., Hedgecock, I. M., and Pirrone, N.: Global atmospheric cycle of mercury: a model study on the impact of oxidation mechanisms, *Environ. Sci. Pollut. R.*, 21, 4110-4123, 2014.
- 1060 De Simone, F., Cinnirella, S., Gencarelli, C. N., Yang, X., Hedgecock, I. M., and Pirrone, N.: Model study of global mercury deposition from biomass burning, *Environ. Sci. Technol.*, 49, 6712-6721, 2015.
- De Simone, F., Cinnirella, S., Gencarelli, C. N., Carbone, F., Hedgecock, I. M., and Pirrone, N.: Particulate-Phase Mercury Emissions during Biomass Burning and Impact on Resulting Deposition: a Modelling Assessment, *Atmos. Chem. Phys. Discuss.*, doi:10.5194/acp-2016-685, in review, 2016.
- 1065 Dibble, T. S., Zelic, M. J., and Mao, H.: Thermodynamics of reactions of ClHg and BrHg radicals with atmospherically abundant free radicals, *Atmos. Chem. Phys.*, 12, 10271-10279, 2012.
- Doms G. 2011. A Description of the Nonhydrostatic Regional COSMO model. Part I: Dynamics and Numerics. Tech. rep., Deutscher Wetterdienst. <http://www.cosmo-model.org/content/model/documentation/core/cosmoDyncsNumcs.pdf>. Accessed 1 July 2016.
- 1070 Doms G, Förstner J, Heise E, Herzog H-J, Mrionow D, et al. 2011. A Description of the Nonhydrostatic Regional COSMO Model. Part II: Physical Parameterization. Tech. rep., Deutscher Wetterdienst. <http://www.cosmo-model.org/content/model/documentation/core/cosmoPhysParamtr.pdf>. Accessed 1 July 2016.
- Donohoue, D. L., Bauer, D., Cossairt, B., and Hynes, A. J.: Temperature and Pressure Dependent Rate Coefficients for the Reaction of Hg with Br and the Reaction of Br with Br: A Pulsed Laser Photolysis-Pulsed Laser Induced Fluorescence Study, *J. Phys. Chem. A*, 110, 6623-6632, doi: 10.1021/jp054688j, 2006.
- 1075 Durnford, D., DByun DW, Ching JKS. 1999. Science Algorithms of the EPA Models-3 Community Multi-scale Air Quality (CMAQ) Modeling System. EPA/600/R-99/030. US EPA National Exposure Research Laboratory. Research Triangle Park, NC.
- Durnford, D., Dastoor, A., Ryzhkov, A., Poissant, L., Pilote, M., and Figueras-Nieto, D.: How relevant is the deposition of mercury onto snowpacks? – Part 2: A modeling study, *Atmos. Chem. Phys.*, 12, 9251-9274, doi:10.5194/acp-12-9251-2012, 2012.
- 1080 ECMWF: European Centre for Medium-Range Weather Forecasts, <http://www.ecmwf.int/en/forecasts/dataset>, access: 1 November 2016
- Emmons, L. K., Walters, S., Hess, P. G., Lamarque, J. F., Pfister, G. G., Fillmore, D., Granier, C., Guenther, A., Kinnison, D., Laepple, T., Orlando, J., Tie, X., Tyndall, G., Wiedinmyer, C., Baughcum, S. L., and Kloster, S.: Description and evaluation of the Model for Ozone and Related chemical Tracers, version 4 (MOZART-4), *Geosci. Model Dev.*, 3, 43-67, doi:10.5194/gmd-3-43-2010, 2010.
- 1085 Foley, K.M., Roselle, S.J., Appel, K.W., Bhawe, P.V., Pleim, J.E., Otte, T.L., Mathur, R., Sarwar, G., Young, J.O., Gilliam, R.C., Nolte, C.G., Kelly, J.T., Gilliland, A.B., Bash, J.O., 2010. Incremental testing of the Community Multiscale Air Quality (CMAQ) modeling system version 4.7. *Geoscientific Model Development*, 3 205-226.
- 1090 2010.
- Fu, X.W., Maruschak, N., Heimbürger, L.-E., Sauvage, B., Ghesi, F., Prestbo, E.M., Sonke, J.E. 2016. Atmospheric mercury speciation dynamics at the high-altitude Pic du Midi. *Atmos. Chem. Phys.*, 16, 5623-5639, 2016. doi:10.5194/acp-16-5623-2016
- 1095 Gay, D., Schmeltz, D., Prestbo, E., Olson, M., Sharac, T., and Tordon, R.: The atmospheric mercury network: measurement and initial examination of an ongoing atmospheric mercury record across North America, *Atmospheric Chemistry and Physics*, 13, 10 521-10 546, 2013.
- Gbor, P. K., Wen, D., Meng, F., Yang, F., Sloan, J. J.: Sloan Modeling of mercury emission, transport and deposition in North America. *Atmos. Environ.*, 41, 1135-49, 2007.
- 1100 Gencarelli, C. N., De Simone, F., Hedgecock, I. M., Sprovieri, F., and Pirrone, N.: Development and application of a regional scale atmospheric mercury model based on WRF/Chem: a Mediterranean area investigation, *Environmental Science and Pollution Research*, 2014a.
- Gencarelli, C. N., Hedgecock, I. M., Sprovieri, F., Schurmann, G. J., and Pirrone, N.: Importance of ship emissions to local summertime ozone production in the mediterranean marine boundary layer: a modeling study, *Atmosphere*, 5(4), 937-958, 2014b.
- 1105 Gencarelli, C.N., Bieser, J., Crabone, F., De Simone, F., Hedgecock, I.M., Matthias, V., Travnikov, O., Yang, X., Pirrone, N., Sensitivity study of regional mercury dispersion in the stmosphere. *Atmos. Chem. Phys. Discuss.*, doi:10.5194/acp-2016-663, 2016 (under review)



- Geyer B. 2014. High-resolution atmospheric reconstruction for Europe 1948–2012: coastDat2. *Earth Syst Sci Data* 6.
- 1110 GMOS: Global Mercury Observation System, Spatial Data Infrastructure, <http://www.gmos.eu/sdi/>, access: 1 November 2016.
- Goodsite, M. E., Plane, J. M. C., and Skov, H. A Theoretical Study of the Oxidation of Hg⁰ to HgBr₂ in the Troposphere. *Environ. Sci. Technol.*, 38, 1772-1776, 2004.
- 1115 Goodsite, M. E., Plane, J. M. C., and Skov, H.: Correction to A Theoretical Study of the Oxidation of Hg⁰ to HgBr₂ in the Troposphere, *Environ. Sci. Technol.*, 46, 5262, 2012.
- Granier, C., Lamarque, J., Mieville, A., Muller, J., Olivier, J., Orlando, J., Peters, J., Petron, G., Tyndall, G., Wallens, S.: POET, a database of surface emissions of ozone precursors, available at <http://www.aero.jussieu.fr/projet/ACCENT/POET.php>, 2005, access: 1 November 2016.
- 1120 Gratz, L.E., Ambrose, J.L., Jaffe, D.A., Shah, V., Jaeglé, L., Stutz, J., Festa, J., Spolaor, M., Tsai, C., Selin, N.E., Song, S., Zhou, X., Weinheimer, A.J., Knapp, D.J., Montzka, D.D., Flocke, F.M., Campos, T.L., Apel, E., Hornbrook, R., Blake, N.J., Hall, S., Tyndall, G.S., Reeves, M., Stechman, D., and Stell, M., 2015. Oxidation of mercury by bromine in the subtropical Pacific free troposphere. *Geophysical Research Letters* 42, 10,494–10,502, doi: 10.1002/2015GL066645.
- 1125 Grell, G. A., Peckham, S. E., Schmitz, R., McKeen, S. A., Frost, G., Skamarock, W. C., and Eder, B.: Fully coupled "online" chemistry within the WRF model, *Atmospheric Environment*, 39, 6957–6975, 2005.
- Gustin MS, Amos HM, Huang J, Miller MB, Heidecorn K. 2015. Measuring and modeling mercury in the atmosphere: A critical review. *Atmos Chem Phys* 15(10): 5697–5713. doi: 10.5194/acp-15-5697-2015.
- Hall, B.: The gas phase oxidation of mercury by ozone. *Water Air Soil Poll.*, 80, 301-315, 1995.
- 1130 Hedgecock, I. M. and Pirrone, N.: Chasing quicksilver: Modeling the atmospheric lifetime of Hg-(g)(0) in the marine boundary layer at various latitudes, *Environmental Science and Technology*, 38, 69-76, 2004.
- Holmes, C. D., Jacob D. J., Mason R. P., Jaffe D. A.: Sources and deposition of reactive gaseous mercury in the marine atmosphere, *Atmospheric Environment* 43(14), 2278-2285, 2009.
- Holmes, C. D., Jacob, D. J., Corbitt, E. S., Mao, J., Yang, X., Talbot, R., and Slemr, F.: Global atmospheric model for mercury including oxidation by bromine atoms, *Atmos. Chem. Phys.*, 10, 12037-12057, 2010.
- 1135 Huang, J., Miller, M.B., Weiss-Penzias, P., Gustin, M.S. 2013. Comparison of Gaseous Oxidized Hg Measured by KCl-Coated Denuders, and Nylon and Cation Exchange Membranes. *Environ. Sci. Technol.*, 2013, 47 (13), pp 7307–7316.
- Huang, J. and Gustin, M.S. 2015. Uncertainties of Gaseous Oxidized Mercury Measurements Using KCl-Coated Denuders, Cation-Exchange Membranes, and Nylon Membranes: Humidity Influences. *Environ. Sci. Technol.*, 2015, 49 (10), pp 6102–6108. doi: 10.1021/acs.est.5b00098
- 1140 Huijnen V, Williams J, van Weele M, van Noije T, Krol M, et al. 2010. The global chemistry transport model TM5: Description and evaluation of the tropospheric chemistry version 3.0. *Geosci Model Dev* 3: 445–473. doi: 10.5194/gmd-3-445-2010.
- 1145 Jaffe DA, Lyman S, Amos HM, Gustin MS, Huang J, et al. 2014. Progress on Understanding Atmospheric Mercury Hampered by Uncertain Measurements. *Environ Sci Technol* 48(13): 7204–7213. doi: 10.1021/es40242a001
1999. Science Algorithms of the EPA Models-3 Community Multi-scale Air Quality (CMAQ) Modeling System. EPA/600/R-99/030. US EPA National Exposure Research Laboratory. Research Triangle Park, NC.
- Janjic, Z. I., 1994: The step-mountain eta coordinate model: further developments of the convection, viscous sublayer and turbulence closure schemes, *Mon. Wea. Rev.*, 122, 927–945.
- 1150 Janjic, Z. I., 2000: Comments on "Development and Evaluation of a Convection Scheme for Use in Climate Models", *J. Atmos. Sci.*, 57, p. 3686.
- Jung, G., Hedgecock, I. M., and Pirrone, N.: ECHMERIT V1.0 - a new global fully coupled mercury-chemistry and transport model, *Geosci. Model Dev.*, 2, 175-195, 10.5194/gmd-2-175-2009, 2009.
- 1155 Kalnay E, Kanamitsu M, Kistler R, Collins W, Deaven D, et al. 1996. The NCEP/NCAR 40-year reanalysis project. *B Am Meteorol Soc* 77: 437–471.
- Kos G, Ryzhkov A, Dastoor A, Narayan J, Steffen A, et al. 2013. Evaluation of discrepancy between measured and modelled oxidized mercury species. *Atmos Chem Phys* 13(9): 4839–4853. doi: 10.5194/acp-13-4839-2013.



- 1160 Lee, D.S., Nemitz, E., Fowler, D., Kingdon, R.D. 2001. Modeling atmospheric transport and deposition across Europe and the UK. *Atmos. Environ.* 35: 5455-5466. doi: 10.1016/S1352-2310(01)00284-9
- Lyman SN, Jaffe DA, Gustin MS. 2010. Release of mercury halides from KCl denuders in the presence of ozone. *Atmos Chem Phys* 10(17): 8197-8204. doi: 10.5194/acp-10-8197-2010.
- 1165 Lyman, S.N., Byun DW, Ching JKS. 1999. Science Algorithms of the EPA Models-3 Community Multi-scale Air Quality (CMAQ) Modeling System. EPA/600/R-99/030. US EPA National Exposure Research Laboratory, Research Triangle Park, NC.
- Lyman, S., Jones, C., O'Neil, T., Allen, T., Miller, M., Gustin, M.S., Pierce, A.M., Luke, W., Ren, X., Kelley, P., 2016. Automated Calibration of Atmospheric Oxidized Mercury Measurements. *Environ. Sci. Technol.*, Article ASAP. doi: 10.1021/acs.est.6b04211
- 1170 Mason, R.: Mercury emissions from natural processes and their importance in the global mercury cycle, in: Mercury fate and transport in the global atmosphere, in: Pirrone, N. and Mason, R. P. (Eds.): *Mercury Fate and Transport in the Global Atmosphere: Emissions, Measurements, and Models*, Springer, pp. 173-191, 2009.
- McClure, C.D., Jaffe, D.A., Edgerton, E.S. 2014. Evaluation of the KCl Denuder Method for Gaseous Oxidized Mercury using HgBr₂ at an In-Service AMNet Site. *Environ. Sci. Technol.*, 2014, 48 (19), pp 11437-11444. doi: 10.1021/es502545k
- 1175 Muntean, M., Janssens-Maenhout, G., Song, S., Selin, N.E., Jos, Oliver, J.G.J., Guizzardi, D., Maas, R., Dentener, F., Trand analysis from 1970 to 2008 and model evaluation of EDGARv4 global gridded anthropogenic mercury emissions. *Science of the Total Environment* 494-495 (2014) 337-350.
- Munthe, J.: The aqueous oxidation of elemental mercury by ozone, *Atmos. Environ.*, 26, 1461-1468, 1992.
- 1180 Olsen, M.A., Schoeberl, M.R., Douglass, A.R. 2004. Stratosphere-troposphere exchange of mass and ozone. *JOURNAL OF GEOPHYSICAL RESEARCH*, VOL. 109, D24114, doi:10.1029/2004JD005186, 2004
- Otte, T. L. and Pleim, J. E.: The Meteorology-Chemistry Interface Processor (MCIP) for the CMAQ modeling system: updates through MCIPv3.4.1, *Geosci. Model Dev.*, 3, 243-256, 2010.
- 1185 Parrella, J. P., Jacob, D. J., Liang, Q., Zhang, Y., Mickley, L. J., Miller, B., Evans, M. J., Yang, X., Pyle, J. A., Theys, N., and Van Roozendaal, M.: Tropospheric bromine chemistry: implications for present and pre-industrial ozone and mercury, *Atmos. Chem. Phys.*, 12, 6723-6740, 2012.
- Petersen, G., Bloxan, R., Wong, S., Munthe, J., Krüger, O., Schmolcke, S.R., Kumar, A.V., 2001. A comprehensive Eulerian modeling framework for airborne mercury species: model development and application in Europe. *Atmos. Environ.* 35: 3063-3074. doi: 10.1016/S1352-2310(01)00110-8
- 1190 Peters, J.A.H.W. and Olivier, J.G.J.: EDGAR3/POET ENUSUIBS; 1997 emissions and scenarios for 1995-2020; technical background information on global and regional sectoral emissions, Report no. 773301003, RIVM, Bilthoven, 2003.
- Pleim, J., Ran, L., 2011. Surface Flux Modeling for Air Quality Applications. *Atmosphere* 2 (3) 271-302.
- 1195 Platt, U. and Janssen, C.: Observation and role of the free radicals NO₃, ClO, BrO and IO in the troposphere, *Faraday Discuss.*, 100, 175-198, 1995.
- Prestbo, E. M. and Gay, D. A.: Wet deposition of mercury in the U.S. and Canada, 1996-2005: Results and analysis of the NADP mercury deposition network (MDN), *Atmospheric Environment*, 43, 4223-4233, 2009.
- Pongprukesa, P., Lin, C.-J., Singhasuk, P., Pan, L., Ho, T.C., Chu, H.W. 2011. Application of CMAQ at a hemispheric scale for atmospheric mercury simulations. *Geosci. Model Dev. Discuss.*, 4, 1723-1754, 2011. doi:10.5194/gmdd-4-1723-2011
- 1200 Qureshi, A., MacLeod, M., Hungerbühler, K. 2011. Quantifying uncertainties in the global mass balance of mercury. *Global Biogeochemical Cycles* 25, GB4012. doi: 10.1029/2011GB004068
- Ritter B, Geleyn JF. 1992. A comprehensive radiation scheme for numerical weather prediction models with potential applications in climate simulations. *Mon Weather Rev* 120: 303-325. doi: 10.1175/1520-0493.
- 1205 Rockel B, Will A, Hense A. 2008. The Regional Climate Model COSMO-CLM (CCLM). *Meteorol Z* 17: 347-248.
- Rutter, A.P., and Schauer, J.J., 2007, The effect of temperature on the gas-particle partitioning of reactive mercury in atmospheric aerosols, *Atmos. Environ.*, 41, 8647-8657.
- Ryaboshapko, A., Bullock, R., Christensen, J., Cohen, M., Dastoor, A., Ilyin, I., Petersen, G., Syrakov, D., Artz, R., Davignon, D., Draxer, R., Munthe, J. 2007. Intercomparison study of atmospheric mercury models, 1.



- 1210 Comparison of models with short-term measurements. *Sci. Total Environ.* 376: 228-240. doi: 10.1016/j.scitotenv.2007.01.072
- Ryaboshapko, A., Bullock, R., Christensen, J., Cohen, M., Dastoor, A., Ilyin, I., Petersen, G., Syrakov, D., Travnikov, O., Artz, R., Davignon, D., Draxer, R., Munthe, J., Pacyna, J. 2007. Intercomparison study of atmospheric mercury models, 2. Modelling results vs. long-term observations and comparison of country deposition budgets. *Sci. Total Environ.* 377: 319-333.
- 1215 Ryaboshapko, A., Bullock, R., Ebinghaus, R., Ilyin, I., Lohman, K., Munthe, J., Petersen, G., Seigneur, I., Wängberg, I. 2002. Comparison of mercury chemistry models. *Atmos. Environ.* 36: 3881-3898. doi: 10.1016/S1352-2310(02)00351-5
- Salzmann, M. and Lawrence, M. G.: Automatic coding of chemistry solvers in WRF-Chem using KPP, in: 7th WRF User's Workshop, Boulder, Colorado, USA, 2006.
- 1220 Sandu, A. and Sander, R.: Technical note: Simulating chemical systems in Fortran90 and Matlab with the Kinetic PreProcessor KPP-2.1, *Atmospheric Chemistry and Physics*, 6, 187–195, doi:10.5194/acp-6-187-2006, 2006.
- Sarwar G, Luecken D, Yarwood G. 2007. Chapter 2.9 Developing and implementing an updated chlorine chemistry into the community multiscale air quality model. *Developments in Environmental Science* 6: 168–176. doi: 10.1016/S1474-8177(07)06029-9.
- 1225 Schaettler U, Doms G, Schraff C. 2008. A Description of the Nonhydrostatic Regional COSMO-Model Part VII: User's Guide. Tech. Rep., Deutscher Wetterdienst.
- Schoerberl, M.R. 2004. Extratropical stratosphere-troposphere mass exchange *JOURNAL OF GEOPHYSICAL RESEARCH*, VOL. 109, D13303, doi:10.1029/2004JD004525, 2004
- 1230 Schrodin R, Heise E. 2001. The multi-layer-version of the DWD soil model TERRA/LM, Tech. Rep, Consortium for Small-Scale Modelling (COSMO). <http://www.cosmo-model.org/content/model/documentation/techReports/docs/techReport02.pdf>. Accessed 1 July 2016.
- Schwede D, Pouliot G, Pierce T. 2005. Changes to the Biogenic Emissions Inventory System Version 3 (BEIS3). Proceedings of the 4th CMAS Models-3 Users' Conference 26–28 September 2005. Chapel Hill, NC.
- 1235 www.cmascenter.org/conference/2005/abstracts/2_7.pdf.
- Seifert A, Beheng KD. 2001. A double-moment parameterization for simulating autoconversion, accretion and selfcollection. *Atmos Res* 59–60:265–281. doi: 10.1016/S0169-8095(01)00126-0.
- Seifert A, Beheng KD. 2006. A two-moment cloud microphysics parameterization for mixed-phase clouds. Part 1: Model description. *Meteorol Atmos Phys* 92:45–66.
- 1240 Seigneur, C., Laramchandani, P., Lohman, K., Vijayaraghavan, K. 2001. Multiscal modeling of the atmospheric fate and transport of mercury. *J. Geophys. Res.* 106: 27795-27809. doi: 10.1029/2000JD000273
- Selin, N.E., Jacob, D.J., Park, R.J., Yantosca, R.M., Strode, S., Jaegle, L., Jaffe, D., 2007. Chemical cycling and deposition of atmospheric mercury: Global constraints from observations. *Journal of Geophysical Research Atmospheres*, 112 D2, 2007. doi: 10.1029/2006JD007450
- 1245 Selin, N.E., Jacob, D. J., Yantosca, R. M., Strode, S., Jaeglé, L., and Sunderland, E. M.: Global 3-D land-ocean-atmosphere model for mercury: present-day versus preindustrial cycles and anthropogenic enrichment factors for deposition, *Global biogeochemical cycles*, 22, doi:10.1029/2007GB003040, 2008.
- Shah, V., Jaeglé, L., Gratz, L.E., Ambrose, J.L., Jaffe, D.A., Selin, N.E., Song, S., Campos, T.L., Flock, F.M., Reeves, M., Stechman, D., Stell, M., Festa, J., Stutz, J., Weinheimer, A.J., Knapp, D.J., Montzka, D.D., Tyndall, G.S., Apel, E.C., Hornbrook, R.S., Hills, A.J., Riemer, D.D., Blake, N.J., Cantrell, C.A., and Mauldin, R.L., III, 2016. Origin of oxidized mercury in the summertime free troposphere over the southeastern US. *Atmospheric Chemistry and Physics* 16, 1511–1530, doi: 10.5194/acp-16-1511-2016.
- 1250 Shetty, S. K., Lin, C.-J., Streets, D. G., Jang, C.: Model estimate of mercury emission from natural sources in East Asia, *Atmos. Environ.*, 42, 8674-8685, 2008.
- 1255 Skamarock, W. C., Klemp, J. B., Dudhia, J., Gill, D. O., Barker, D. M., Wang, W., Powers, J. G.: A description of the Advanced Research WRF Version 2. NCAR/TN-468+STR.. NCAR Technical Note. Boulder, CO, USA, 2007.
- Slemr, F., Weigelt, A., Ebinghaus, R., Kock, H.H., Bödewadt, J., Brenninkmeijer, C.A.M., Rauthe-Schöch, A., Weber, S., Hermann, M., Zahn, A., Martinsson, B. 2016. Atmospheric mercury measurements onboard the CARIBIC passenger aircraft. *Atmos. Meas. Tech. Discuss.*, doi:10.5194/amt-2015-376, 2016
- 1260



- Slemr, F., Weigelt, A., Ebinghaus, R., Brenninkmeijer, C., Baker, A., Schuck, T., Rauthe-Schöch, A., Riede, H., Leedham, E., Hermann, M. Van Velthoven, P., Oram, D., O'sullivan, D., Dyroff, C., Zahn, A., Ziereis, H. 2014. Mercury Plumes in the Global Upper Troposphere Observed during Flights with the CARIBIC Observatory from May 2005 until June 2013. *Atmosphere* 2014, 5, 342-369. doi:10.3390/atmos5020342
- 1265 Soerensen, A. L., Sunderland, E. M., Holmes, C. D., Jacob, D. J., Yantosca, R. M., Skov, H., Christensen, J. H., Strode, S. A., and Mason, R. P.: An improved global model for air-sea exchange of mercury: high concentrations over the north atlantic, *Environmental Science and Technology*, 44, 8574-8580, 2010.
- Sommar, J., Gärdfeldt, K., Strömberg, D., and Feng, X.: A kinetic study of the gas-phase reaction between the hydroxyl radical and atomic mercury, *Atmos. Environ.*, 35, 3049-3054, 2001.
- 1270 Song, S., Soerenson, A.L., Angot, H., Artz, R., Brooks, S., Brunke, E.-G., Conley, G., Dommergue, A., Ebinghaus, R., Holsen, T.M., Ja, D. A., Kang, S., Kelley, P., Luke, W. T., Magand, O., Marumoto, K., Pfaffenhuber, K.A., Ren, X., Sheu, G.-R., Slemr, F., Warneke, T., Weigelt, A., Weiss-Penzias, P., Wip, D. C., Zhang, Q. 2015. Top-down constraints on atmospheric mercury emissions and implications for global. *Atmos. Chem. Phys. Discuss.*, 15, 5269–5325, 2015. doi:10.5194/acpd-15-5269-2015
- 1275 Sprenger, M., Maspoli, M.C., Wernli, H. 2003. Tropopause folds and cross-tropopause exchange: A global investigation based upon ECMWF analyses for the time period March 2000 to February 2001. *JOURNAL OF GEOPHYSICAL RESEARCH*, VOL. 108, NO. D12, 8518, doi:10.1029/2002JD002587, 2003
- Sprenger, M. and Wernli, H.,. 2003. A northern hemispheric climatology of cross-tropopause exchange for the ERA15 time period (1979–1993). *JOURNAL OF GEOPHYSICAL RESEARCH*, VOL. 108, NO. D12, 8521, doi:10.1029/2002JD002636, 2003
- 1280 Sprovieri, F. and Pirrone, N. and Bencardino, M. and D'Amore, F. and Carbone, F. and Cinnirella, S. and Mannarino, V. and Landis, M. and Ebinghaus, R. and Weigelt, A. and Brunke, E.-G. and Labuschagne, C. and Martin, L. and Munthe, J. and Wängberg, I. and Artaxo, P. and Morais, F. and Barbosa, H. D. M. J. and Brito, J. and Cairns, W. and Barbante, C. and Dieguez, M. D. C. and Garcia, P. E. and Dommergue, A. and Angot, H. and Magand, O. and Skov, H. and Horvat, M. and Kotnik, J. and Read, K. A. and Neves, L. M. and Gawlik, B. M. and Sena, F. and Mashyanov, N. and Obolkin, V. and Wip, D. and Feng, X. B. and Zhang, H. and Fu, X. and Ramachandran, R. and Cossa, D. and Knoery, J. and Maruszczak, N. and Nerentorp, M. and Norstrom, C. 2016. Atmospheric mercury concentrations observed at ground-based monitoring sites globally distributed in the framework of the GMOS network. *Atmos. Chem. Phys.*, 16, 11915-11935, 2016. doi:10.5194/acp-16-11915-2016
- 1290 Sprung, D., and Zahn, A. 2010. Acetone in the upper troposphere/lower stratosphere measured by the CARIBIC passenger aircraft: Distribution, seasonal cycle, and variability. *J. Geophys. Res.* 115, D16301, doi:10.1029/2009JD012099.
- 1295 Steppeler J, Doms G, Schattler U, Bitzer HW, Gassmann A, et al. 2003. Meso-gamma scale forecasts using the nonhydrostatic model LM. *Meteorol Atmos Phys* 82: 75–96. doi: 10.1007/s00703-001-0592-9.
- Strode SA, Jaegle L, Selin N, Jacob D, Park R, et al. 2007. Air-sea exchange in the global mercury cycle. *Global Biogeochem Cy* 21. doi: 10.1029/2006 GB002766.
- Tanaka PL, Allen DT, McDonald-Buller EC, Chang S, Kimura Y, et al. 2003. Development of a chlorine mechanism for use in the carbon bond IV chemistry model. *J Geophys Res-Atmos* 108. doi: 10.1029/2002JD002432.
- 1300 Tiedtke M. 1989. A comprehensive mass flux scheme for cumulus parameterization in large-scale models. *Mon Weather Rev* 117: 1779–1800. doi: 10.1175/1520-0493(1989)117.
- Thompson, G., R. M. Rasmussen, and K. Manning, 2004: Explicit forecasts of winter precipitation using an improved bulk microphysics scheme. Part I: Description and sensitivity analysis. *Mon. Wea. Rev.*, 132, 519–542.
- 1305 Tørseth, K., Aas, W., Breivik, K., Fjæraa, A. M., Fiebig, M., Hjellbrekke, A. G., Lund Myhre, C., Solberg, S., and Yttri, K. E.: Introduction to the European Monitoring and Evaluation Programme (EMEP) and observed atmospheric composition change during 1972–2009, *Atmos. Chem. Phys.*, 12, 5447-5481, doi:10.5194/acp-12-5447-2012, 2012
- 1310 Tossell, J. A.: Calculation of the energetics for oxidation of gas-phase elemental Hg by Br and BrO, *J. Phys. Chem. A*, 107, 7804-7808, 2003.



- Travnikov, O. 2005. Contribution of the intercontinental atmospheric transport to mercury pollution in the Northern Hemisphere. *Atmos. Environ.* 39, 7541-7548, 2005.
- 1315 Travnikov, O. and Ilyin, I.: The EMEP/MSC-E Mercury Modeling System, in: Pirrone, N. and Mason, R. P. (Eds.): *Mercury Fate and Transport in the Global Atmosphere: Emissions, Measurements, and Models*, Springer, pp. 571-587, 2009.
- Travnikov, O., Jonson, J. E., Andersen, A. S., Gauss, M., Gusev, A., Rozovskaya, O., Simpson, D., Sokovyh, V., Valiyaveetil, S., and Wind, P.: Development of the EMEP global modelling framework: Progress report. EMEP/MSC-E Technical Report 7/2009, Meteorological Synthesizing Centre - East of EMEP, Moscow, 44 pp., available: <http://www.msceast.org/index.php/publications/reports>
- 1320 Travnikov, O., Lin, C. J., Dastoor, A., Bullock, O. R., Hedgecock, I., Holmes, C., Ilyin, I., Jaegle, L., Jung, G., Pan, L., Pongprueksa, P., Ryzhkov, A., Seigneur, C., and Skov, H.: Global and Regional Modeling, 2010. in: Pirrone, N. and T. Keating, *Hemispheric Transport of Air Pollution 2010, Part B: Mercury, Air Pollution Studies No. 16*. United Nations, 97-144, 2010.
- 1325 Travnikov, O. and Angot, H. and Artaxo, P. and Bencardino, M. and Bieser, J. and D'Amore, F. and Dastoor, A. and De Simone, F. and Dieguez, M. D. C. and Dommergue, A. and Ebinghaus, R. and Feng, X. B. and Gencarelli, C. N. and Hedgecock, I. M. and Magand, O. and Martin, L. and Matthias, V. and Mashyanov, N. and Pirrone, N. and Ramachandran, R. and Read, K. A. and Ryzhkov, A. and Selin, N. E. and Sena, F. and Song, S. and Sprovieri, F. and Wip, D. and Wängberg, I. and Yang, X. 2016. Multi-model study of mercury dispersion in the atmosphere: Atmospheric processes and model evaluation. *ACPD*. doi:10.5194/acp-2016-924
- 1330 UNEP, 2013. The Minamata Convention on Mercury, available at: <http://www.mercuryconvention.org/Convention/tabid/3426/Default.aspx> (last access: 1 November 2016).
- Van Loon, L., Mader, E., Scott, S. L.: Reduction of the aqueous mercuric ion by sulfite: UV spectrum of HgSO and its intramolecular redox reaction. *J. Phys. Chem. A*, 104, 1621-1626, 2000.
- 1335 Vukovich, J. and T. Pierce (2002) "The Implementation of BEIS3 within the SMOKE Modeling Framework", In Proceedings of the 11th International Emissions Inventory Conference, Atlanta, Georgia, April 15-18, 2002. (Available online: www.epa.gov/ttn/chieff/conference/ei11/modeling/vukovich.pdf)
- 1340 Wang, K., Zhang, Y., Jang, C., Phillips, S., and Wang, B.: Modeling intercontinental air pollution transport over the trans-Pacific region in 2001 using the Community Multiscale Air Quality modeling system, *J. Geophys. Res.*, 114, D04307, doi:10.1029/2008JD010807, 2009
- Wang, X., Lin, C.-J., and Feng, X.: Sensitivity analysis of an updated bidirectional air-surface exchange model for elemental mercury vapor, *Atmos. Chem. Phys.*, 14, 6273–6287, doi:10.5194/acp-14-6273-2014, 2014.
- 1345 Weigelt, A., Ebinghaus, R., Pirrone, N., Bieser, J., Bödewadt, J., Eposito, G., Slemr, F., Van Velthoven, P.F.J., Zahn, A., Ziereis, H. 2016a. Tropospheric mercury vertical profiles between 500 and 10 000 m in central Europe. *Atmos. Chem. Phys.*, 16, 4135–4146. doi:10.5194/acp-16-4135-2016
- Weigelt, A., 2016. Mercury emissions of a coal-fired power plant in Germany. *Atmospheric Chemistry and Physics* 16(21):13653-13668. doi: 10.5194/acp-16-13653-2016
- 1350 Weigelt, A., Ebinghaus, R., Manning, A.J., Derwent, R.G., Simmonds, P.G., Spain, T.G., Jennings, S.G., Slemr, F. 2015. Analysis and interpretation of 18 years of mercury observations since 1996 at Mace Head, Ireland. *Atmospheric Environment* 100 (2015) 83-93.
- Weigelt, A., Temme, C., Bieber, E., Schwerin, A., Schurtze, M., Ebinghaus, R., Kock, H.H. 2013. Measurements of atmospheric mercury species at a German rural background site from 2009 to 2011-methods and results. *Environmental Chemistry* 10(2):102–110.
- 1355 Weiss-Penzias, P., Amos, H.M., Selin, N.E., Gustin, M.S., Jaffe, D.A., et al. 2015. Use of a global model to understand speciated atmospheric mercury observations at five high-elevation sites. *Atmos Chem Phys* 15(3): 1161–1173. doi: 10.5194/acp-15-1161-2015
- Wesely, M. L.: Parameterization of surface resistances to gaseous dry deposition in regional-scale numerical models, *Atmos. Environ.*, 23, 1293-1304, doi:10.1016/0004-6981(89)90153-4, 1989.
- 1360 Wesely, M. L. and Hicks, B.B.: A review of the current status of knowledge on dry deposition. *Atmos. Environ.* 34, 2261-22, 2000.
- Whitten, G.Z., Heo, G., Kimura, Y., McDonald-Buller, E., Allen, D.T., et al. 2010. A new condensed toluene mechanism



- for Carbon Bond: CB05-TU. *Atmos Environ* 44: 5346–5355.
- 1365 Xu, X., Yang, X., Miller, D.R., Helble, J.J., Carley, R.J. 2000. A regional scale modeling study of atmospheric transport and transformation of mercury. I. Model development and evaluation. *Atmos. Environ.* 24 4933-4944. doi: 10.1016/S1352-2310(00)00228-4
- Yang, X., Cox, R., Warwick, N., Pyle, J., Carver, G., O'Connor, F., Savage, N.: Tropospheric bromine chemistry and its impacts on ozone: A model study, *J. Geophys. Res.*, 110, D23311, 2005.
- 1370 Yang, X., Pyle, J. A., Cox, R. A., Theys, N., and Van Roozendaal, M.: Snow-sourced bromine and its implications for polar tropospheric ozone, *Atmos. Chem. Phys.*, 10, 7763-7773, doi:10.5194/acp-10-7763-2010, 2010.
- Yarwood G, Rao S, Yocke M, Whitten GZ. 2005. Updates to the Carbon Bond Mechanism: CB05. Report to the U.S. Environmental Protection Agency. RT-04-00675. <http://www.camx.com/publ/pdfs/>.
- 1375 Zanis, P., Gerasopoulos, E., Priller, A., Schnabel, C., Stohl, A., Zerefos, C., Gäggeler, H.W., Tobler, T., Kubik, P.W., Kanter, H.J., Scheel, H.E., Luterbacher, J., Berger, M. 2003. An estimate of the impact of stratosphere-to-troposphere transport (STT) on the lower free tropospheric ozone over the Alps using ¹⁰Be and ⁷Be measurements. *JOURNAL OF GEOPHYSICAL RESEARCH*, VOL. 108, NO. D12, 8520, doi:10.1029/2002JD002604, 2003
- Zhang, L.: A size-segregated particle dry deposition scheme for an atmospheric aerosol module, *Atmos. Environ.*, 35, 549-560, doi:10.1016/S1352-2310(00)00326-5, 2001.
- 1380 Zhang, L., Brook, J. R., and Vet, R.: A revised parameterization for gaseous dry deposition in air quality models, *Atmos. Chem. Phys.*, 3, 1777-1804, doi:10.5194/acpd-3-1777-2003, 2003.
- Zhang, L., Wright, L. P., Blanchard, P. A: Review of Current Knowledge Concerning Dry Deposition of Atmospheric Mercury, *Atmos. Environ.*, 43, 5853-5864, 2009.
- 1385 Zhang, Y., Jaeglé L., van Donkelaar, A., Martin, R. V., Holmes, C. D., Amos, H. M., Wang, Q., Jacob, D. J., Talbot, R., Artz, R., Holson, T. M., Felton, D., Miller, E. K., Perry, K. D., Schmeltz, D., Steffen, A., and Tordon, R.: Nested-grid simulation of mercury over North America, *Atmos. Chem. Phys.*, 6095-6111, doi:10.5194/acp-12-6095-2012, 2012
- 1390 Zhu, J. Wang, T., Bieser, J., Matthias, V. 2015. Source attribution and process analysis for atmospheric mercury in East China simulated by CMAQ-Hg. *Atmos. Chem. Phys.* 15 (7) 10389-10424.



	GLEMOS	GEOS-CHEM	GEM-MACH-Hg	ECHMERIT	CMAQ-Hem	WRF-CHEM	CCLM-CMAQ
Spatial resolution Scope Horizontal Vertical	Global 1° x 1° 20 levels, top 10 hPa	Global 2.5° x 2° 47 levels, top 0.01 hPa	Global 1° x 1° 58 levels, top 7 hPa	Global T42 (~ 2.8° x 2.8°) 19 levels, top 10hPa	Hemispheric 108 x 108 km ² 13 levels, top 50 hPa	Regional 24 x 24 km ² 30 levels, top 50 hPa	Regional 24 x 24 km ² 30 levels, top 50 hPa
Meteorology Data support type Meteorologica l driver	off-line WRF 3.7.2 / ECMWF	off-line GEOS-FP	on-line GEM	on-line ECHAM5	off-line WRF 3.7 / NCEP	on-line WRF 3.4 / NCEP	off-line CCLM 4.8 / NCEP
Anthropogenic emissions Emission inventory Average speciation GEM : GOM : PBM	AMAP 81 : 15 : 4	AMAP 71 : 19 : 0	AMAP 96 : 3 : 1	AMAP 81 : 15 : 4	AMAP 87 : 10 : 3	AMAP	AMAP 94 : 1 : 5
Natural emissions					-		Bash et al.,
Boundary conditions mercury other species	- -	- -	- -	-	GEOS-Chem GEOS-Chem	ECHMERIT MOZART-4	GLEMOS TM-5
BASE chemistry gas phase aqueous phase reduction processes	Ozone, OH HOCL/OCL yes	Bromine OH no	OH, Bromine ^(a) - no	Ozone, OH Ozone, OH no	Ozone, OH Ozone, OH yes	Ozone, OH Ozone, OH no	Ozone, OH Ozone, OH yes
References	Travnikov and Ilyin	Holmes et al. (2010);	Durnford et al (2012);	Jung et al. (2009); De	Byun and Chang	Grell et al. (2005);	Byun and Chang



	(2009); Travnikov et al. (2009)	Amos et al. (2012); Song et al. (2015)	Kos et al. (2013); Dastoor et al. (2015)	Simone et al. (2014)	(1999); Byun and Schere (2006); Bullock and Brehme (2002); Bullock et al. (2006); Pongprueksa et al. (2011)	Gencarelli et al., (2014; 2015)	(1999); Byun and Schere (2006); Bullock and Brehme (2002); Bullock et al. (2006); Bash et al. (2010); Bieser et al. (2015)
--	------------------------------------	---	---	----------------------	--	---------------------------------	---

Table 1: Model description

Name	Anthropogenic emissions	Gas-phase chemistry	Description
BASE	UNEP2010	Model standard configuration	Base run
NOANT	No emissions	Model standard configuration	Effect of anthropogenic emissions
ANTSPEC	UNEP2010, 100% GEM	Model standard configuration	Effect of emission speciation
NOCHEM	UNEP2010	No chemistry	Effect of chemistry
OHCHEM	UNEP2010	GEM oxidation by OH	OH dataset from MOZART
O3CHEM	UNEP2010	GEM oxidation by O3	O3 dataset from MOZART
BRCHEM1	UNEP2010	GEM oxidation by Br	Br dataset from GEOS-Chem
BRCHEM2	UNEP2010	GEM oxidation by Br	Br dataset from p-TOMCAT

Table 2: Specification of model experiments



Figure 1: Idealized observed TM and GEM mercury profiles for winter, spring, and summer in northern mid-latitudes.

Figure 2: Upper panel: GEM/TGM profiles at Leipzig, Germany (21st August 2013) compiled from ETMEP and
1400 CARIBIC measurements (Weigelt et al., 2016). Lower panel: GEM/TGM profiles at Mace Head, Ireland (19th
September 2013) compiled from GMOS ground based observations (Weigelt et al., 2015) and CARIBIC
measurements (Slemr et al., 2016). Solid lines indicate total mercury (TM), dashed lines indicate elemental
mercury (GEM), and dotted lines depict the GEM/TM ratio given on the second x-axis. The horizontal gray
lines depict PBL and tropopause height. The black squares are ETMEP measurements, the gray circles are
1405 tropospheric and the gray squares are stratospheric CARIBIC measurements.

Figure 3 Comparison of modelled average mercury profile for Europe to observations based on vertical profiles
from ETMEP and CARIBIC campaigns amended with ground based observations at Waldhof and Mace Head
(Weigelt et al., 2013; Slemr et al., 2016). The error bars indicate the 66% quantile range of the observations in
1410 each altitude, the sample size for each altitude is indicated on the y-axis of the legend.

Figure 4: Comparison of modelled average mercury profile for North America to observations based on vertical
profiles at Tullahoma, TN from January and February 2013 (Brooks et al., 2014). The error bars indicate the
66% quantile range of the observations in each altitude, the sample size for each altitude is indicated on the y-
1415 axis of the legend.

Figure 5: Comparison of modelled average mercury profiles for North America to observations based on
NOMADSS flights in June and July 2013 (Shah et al., 2015; Gratz et al., 2016). The error bars indicate the 66%
quantile range of the observations in each altitude, the sample size for each altitude is indicated on the y-axis of
1420 the legend.

Figure 6: Comparison of modelled average mercury profile for North America to observations based on vertical
profiles at Tullahoma, TN from April to June 2013 (Brooks et al., 2014). The error bars indicate the 66%
quantile range of the observations in each altitude, the sample size for each altitude is indicated on the y-axis of
1425 the legend.

Figure 7: GOM profiles at Waldhof Germany (23rd August 2013) (Weigelt et al., 2016). The observations are a
combination of ground based measurements and a total column measurement in altitudes from 500m to 3000m.
Model values are given for BASE (solid line), ANTSPEC (dashed line), NOCHEM (dotted line).



1430

Fig. 8: Comparison of modelled average reactive mercury profiles ($RM = GOM + PBM$) with observations at Tullahoma, TN for January and February 2013 reported by Brooks et al. (2014). The errorbars indicate the 66% quantile range of the observations in each altitude, the sample size for each altitude is indicated on the y-axis of the legend.

1435

Fig. 9: Comparison of average reactive mercury profiles ($RM = GOM + PBM$) at Tullahoma, TN for April, May, and June (Brooks et al., 2014). The errorbars indicate the 66% quantile range of the observations in each altitude, the sample size for each altitude is indicated on the y-axis of the legend.

1440

Figure 10: Comparison of modelled average reactive mercury ($RM = GOM$) concentration to observations based on NOMADSS flights in June and July 2013 (Shah et al., 2015; Gratz et al., 2016). The errorbars indicate the 66% quantile range of the observations in each altitude, the sample size for each altitude is indicated on the y-axis of the legend.

1445

Figure 11: Seasonal vertical profiles of modeled GEM/TM ratios for winter (upper panel) and summer (lower panel). Observations are based on TM and GEM measurements from CARIBIC flights.

Figure 12: Average inter-hemispheric transects for 19 flights from Munich to Sao Paulo. TGM was measured on the outward and GEM on return flights (Slemr et al., 2014). Error bars indicate the 66% quantile range of all observations for a given latitude. Plots in the left column are for TGM and those on the right for GEM.

1450

Figure 13: Relative inter-hemispheric transects for 19 flights from Munich to Sao Paulo. TM (left side) was measured on the outward and GEM (right side) on return flights (Slemr et al., 2014). Error bars indicate the 66% quantile range of all observations for a given latitude. Plot in the left column are for TGM and in the right side for GEM.

1455

Figure 14: Average inter-hemispheric transects for 19 flights from Munich to Sao Paulo. TM (left side) was measured on the outward and GEM (right side) on return flights (Slemr et al., 2014). Error bars indicate the 66% quantile range of all observations for a given latitude.

1460

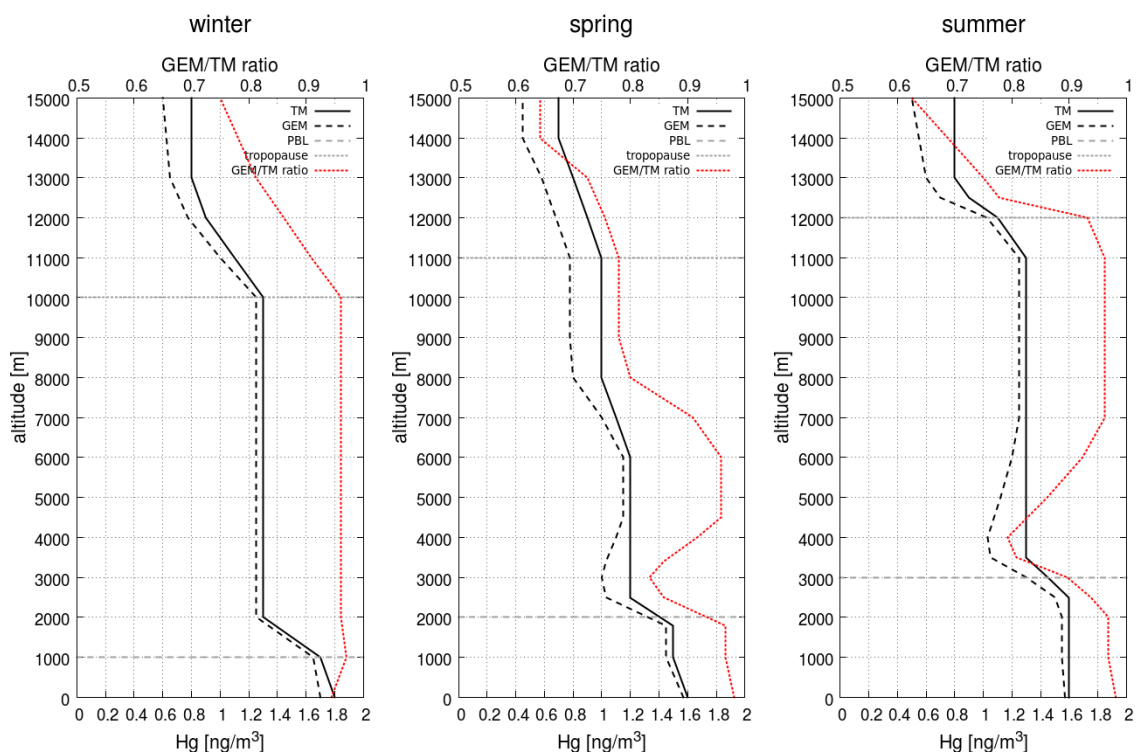


Fig. 1

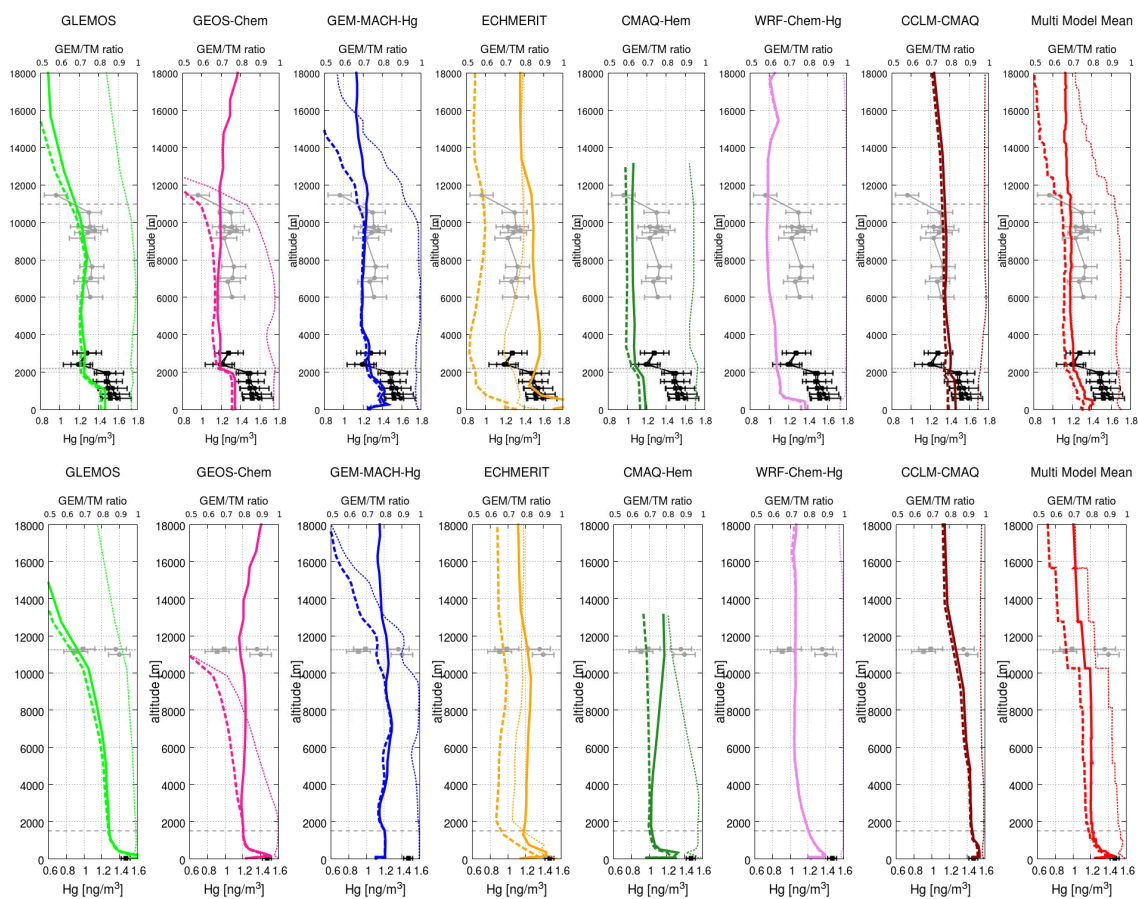


Fig. 2

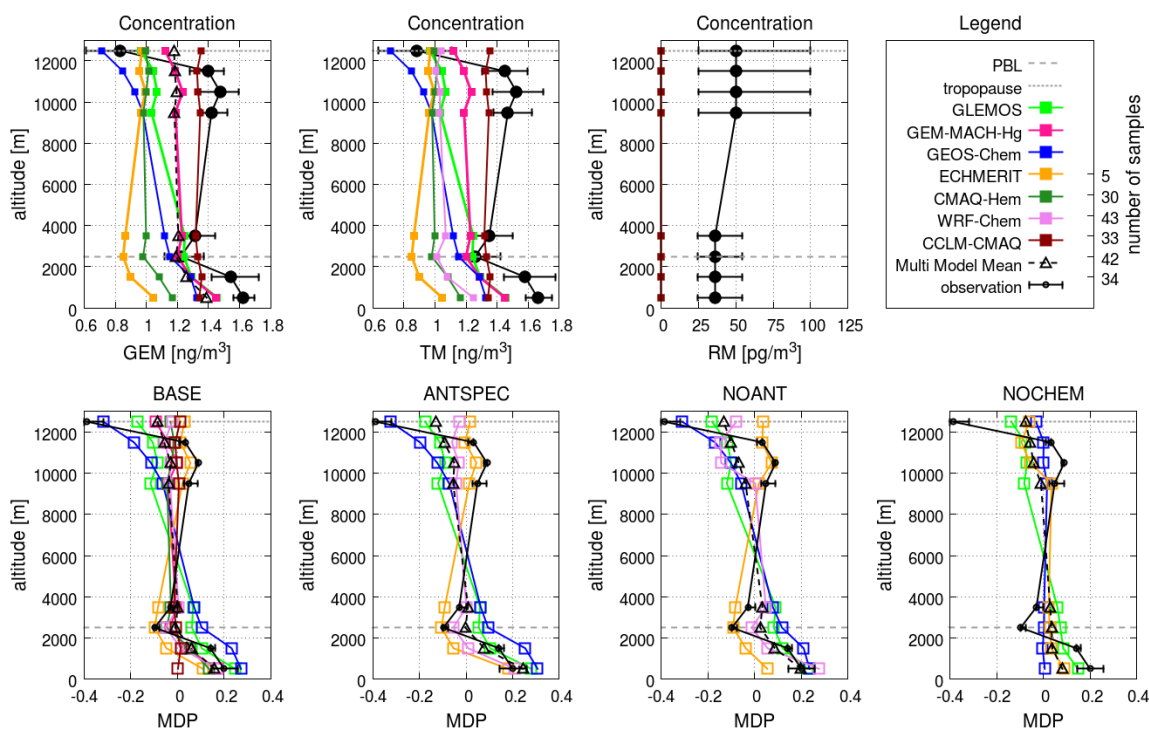
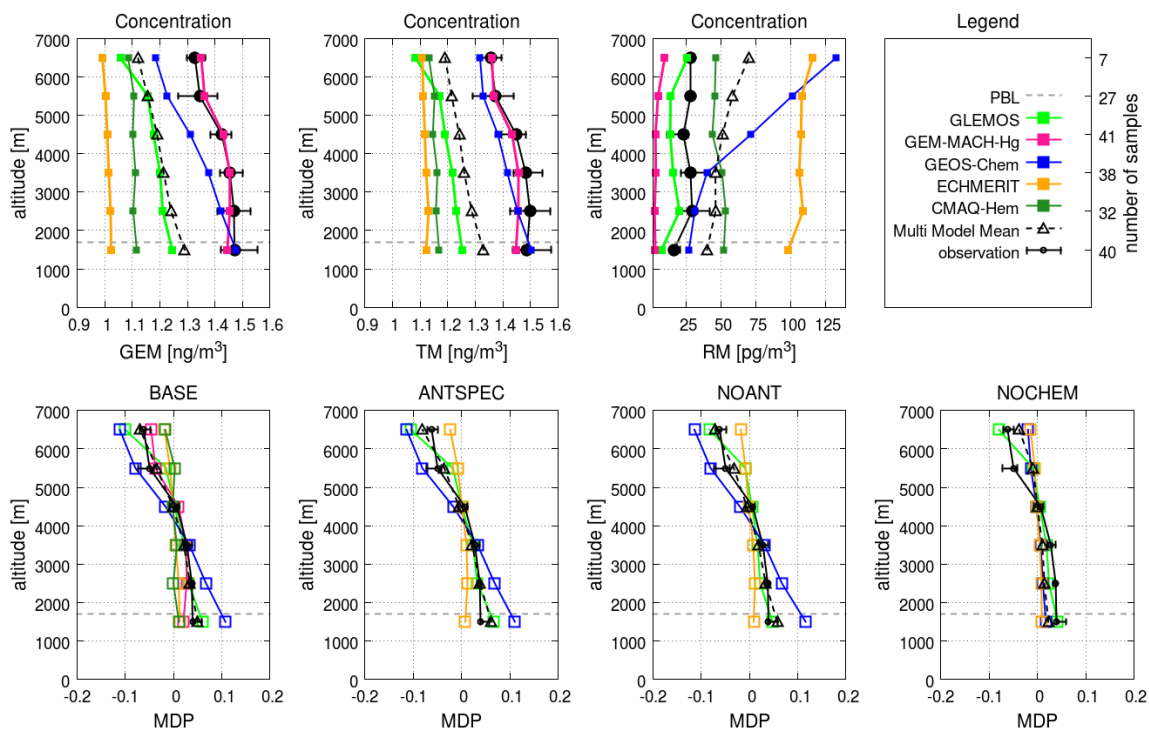


Fig. 3



1465 Fig. 4

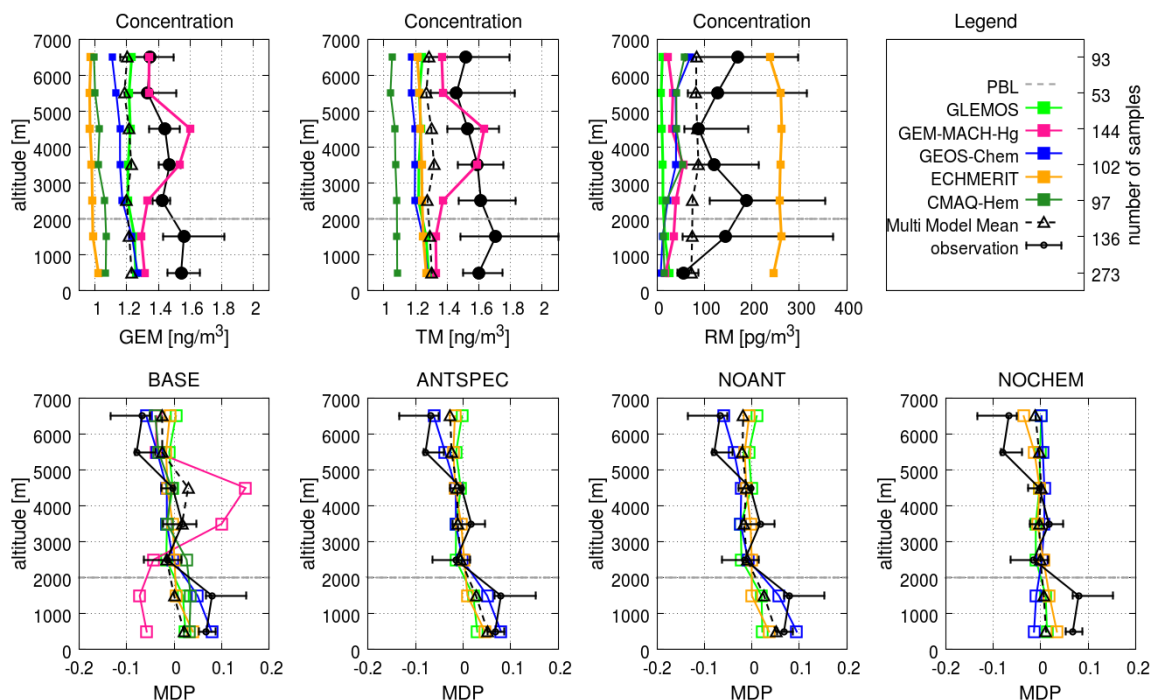


Fig. 5

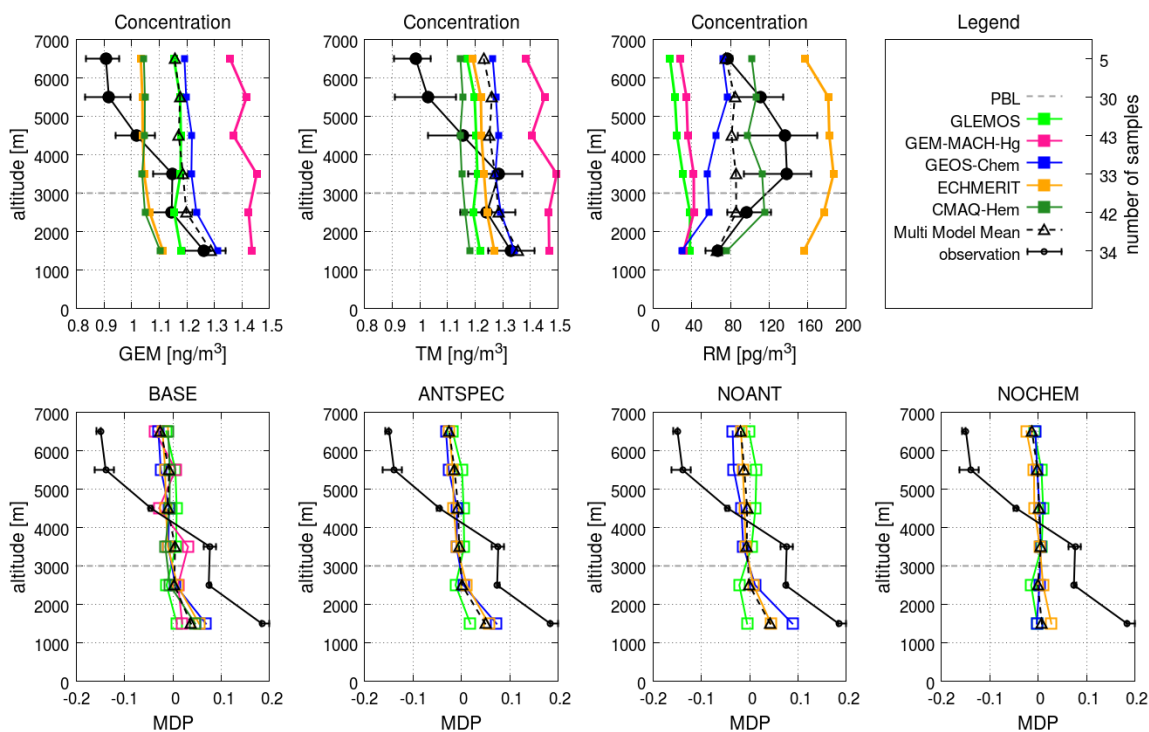


Fig. 6

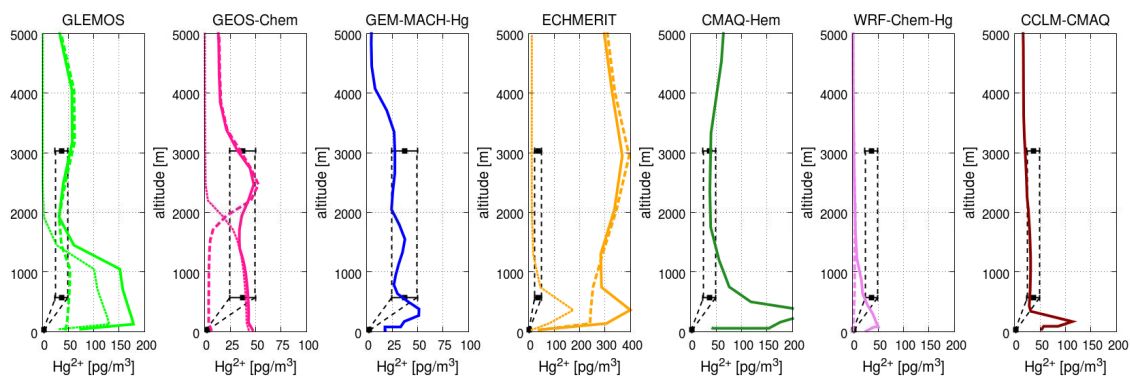


Fig. 7

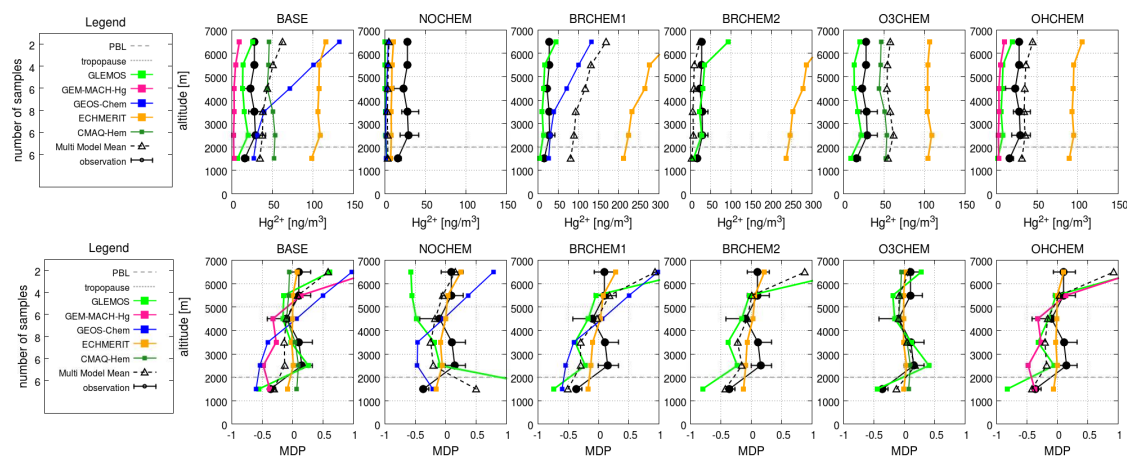
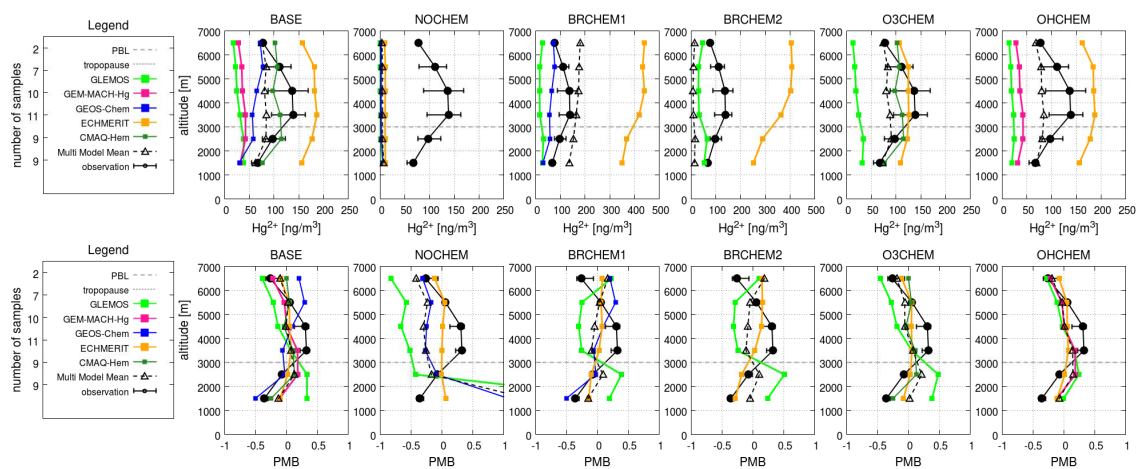


Fig. 8



1470 Fig. 9

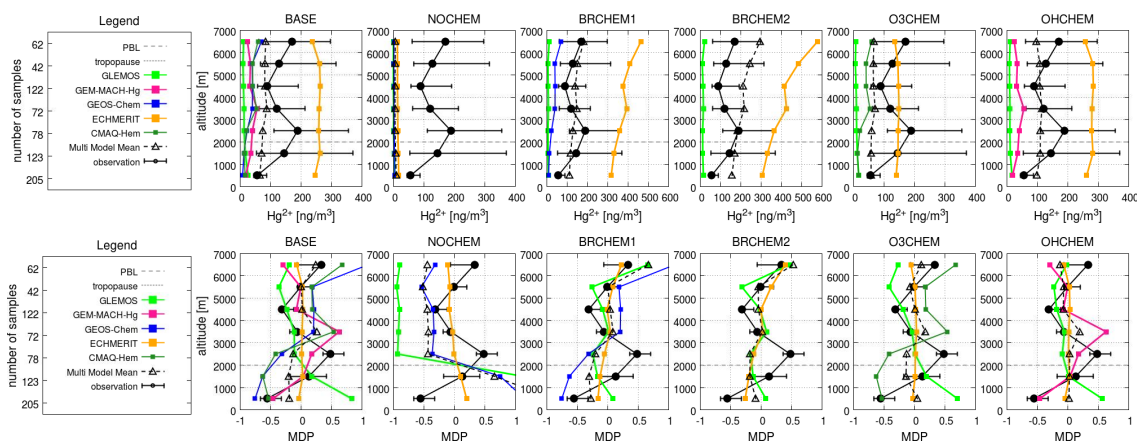


Fig. 10

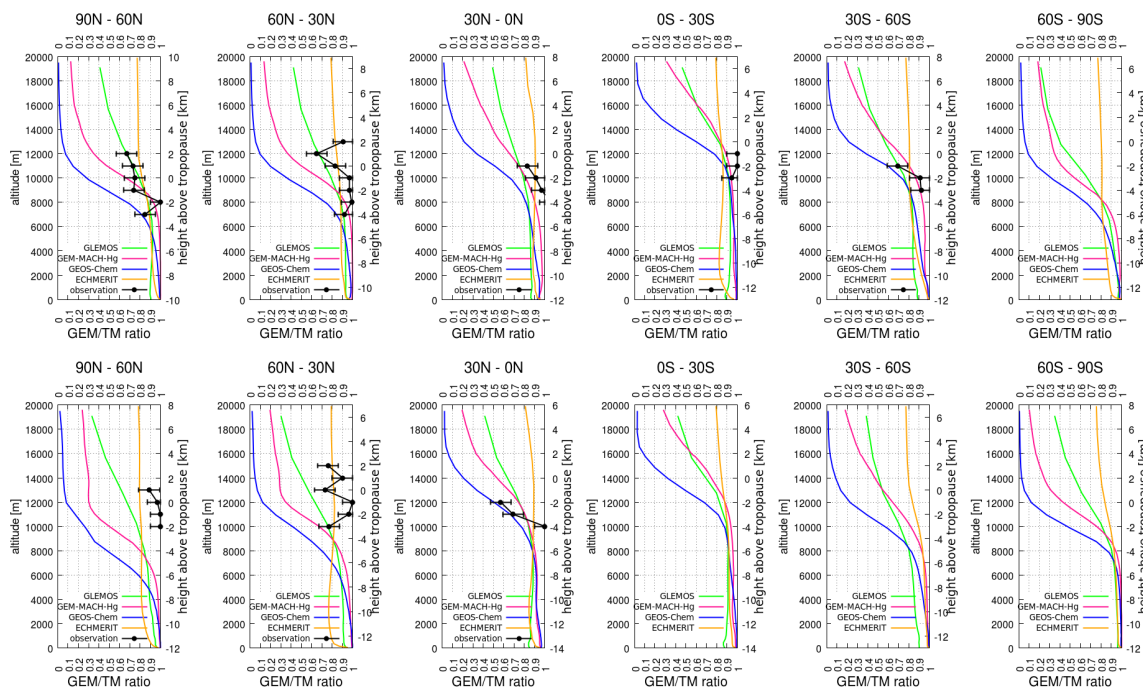


Fig. 11

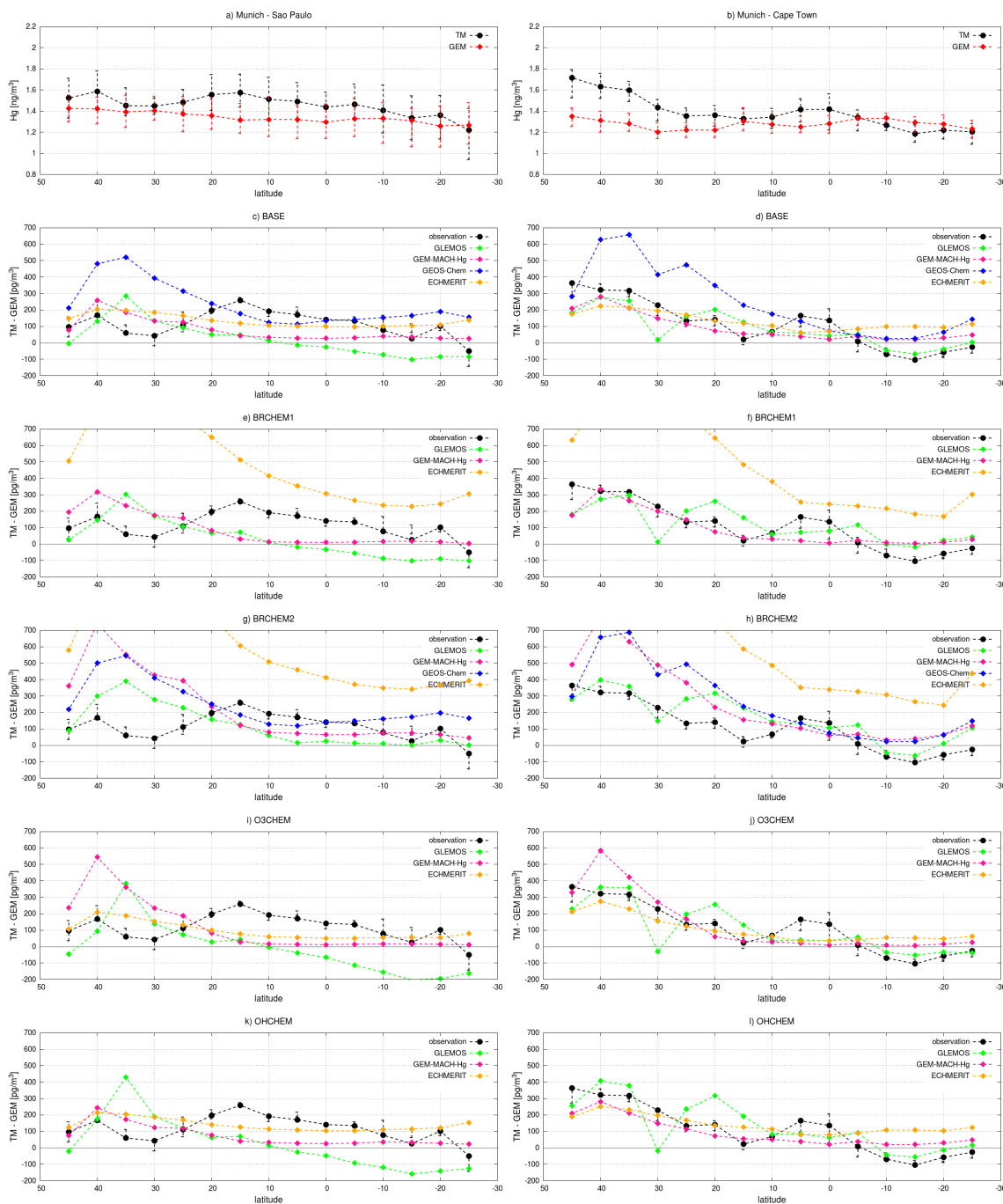


Fig. 12

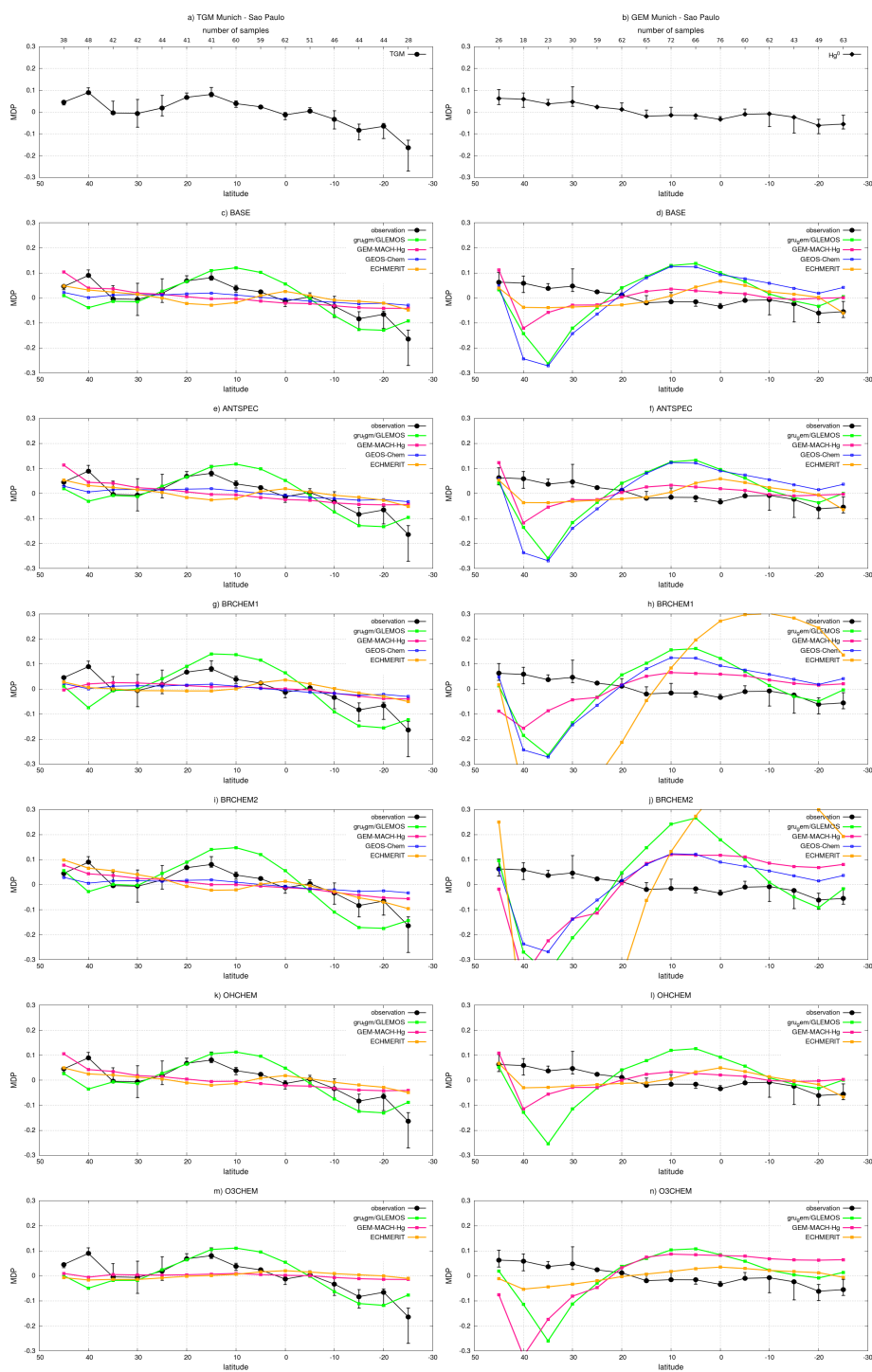
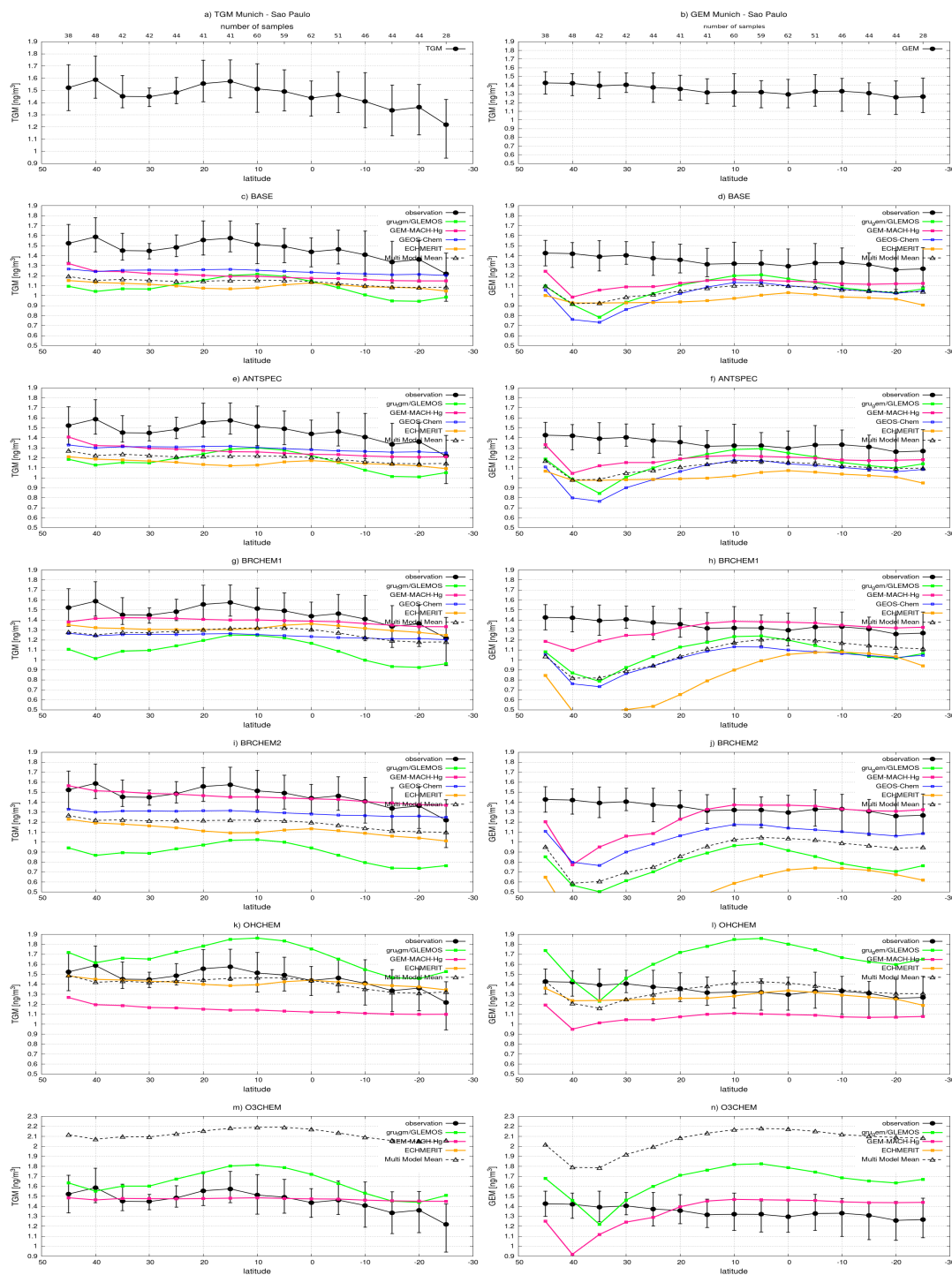


Fig. 13



1475 Fig. 14